UCRL-10450

University of California

Ernest O. Lawrence Radiation Laboratory

TWO-WEEK LOAN COPY

This is a Library Circulating Copy which may be borrowed for two weeks. For a personal retention copy, call Tech. Info. Division, Ext. 5545

Berkeley, California

DISCLAIMER

This document was prepared as an account of work sponsored by the United States Government. While this document is believed to contain correct information, neither the United States Government nor any agency thereof, nor the Regents of the University of California, nor any of their employees, makes any warranty, express or implied, or assumes any legal responsibility for the accuracy, completeness, or usefulness of any information, apparatus, product, or process disclosed, or represents that its use would not infringe privately owned rights. Reference herein to any specific commercial product, process, or service by its trade name, trademark, manufacturer, or otherwise, does not necessarily constitute or imply its endorsement, recommendation, or favoring by the United States Government or any agency thereof, or the Regents of the University of California. The views and opinions of authors expressed herein do not necessarily state or reflect those of the United States Government or any agency thereof or the Regents of the University of California.

Submitted to Annals of Physics

UCRL-10450

UNIVERSITY OF CALIFORNIA

Lawrence Radiation Laboratory
Berkeley, Calkfornia

Contract No. W-7405-eng-48

THE DEFORMATION ENERGY OF A CHARGED DROP: PART V: RESULTS OF ELECTRONIC COMPUTER STUDIES

Stanley Cohen and Wladyslaw J. Swiatecki

August 30, 1962

THE DEFORMATION ENERGY OF A CHARGED DROP: PART V: RESULTS OF ELECTRONIC COMPUTER STUDIES

Stanley Cohen

Argonne National Laboratory
Argonne, Illinois

and

Wladyslaw J. Swiatecki

Lawrence Radiation Laboratory
University of California
Berkeley, California

August 30, 1962

ABSTRACT

The results of electronic machine studies of equilibrium configurations of an idealized charged drop are presented. The symmetric family of saddle-point shapes has been traced as a function of the fissionability parameter x. The properties of the saddle-point shapes have been tabulated in the interval $x = 0.30$ to $x = 1.00$ in steps of 0.02. The appearance of these shapes changes from dumbbell-like for $x \lesssim 0.67$ to cylinder-like for $x \gtrsim 0.67$. The transition is fairly rapid, but not discontinuous. The properties tabulated include the energies, moments of inertia and quadrupole moments of the saddle-point shapes. In addition, the elastic constants (stiffnesses) of the symmetric saddle-point shapes for different types of symmetric and asymmetric distortions have been determined. The shapes were found to be stable against asymmetry down to $x = 0.39_4$, at which point an asymmetric family of equilibrium shapes bifurcates.

A simple formula is given which reproduces the calculated liquid-drop thresholds with fair accuracy.

THE DEFORMATION ENERGY OF A CHARGED DROP: PART V: RESULTS OF ELECTRONIC COMPUTER STUDIES

Stanley Cohen

Argonne National Laboratory
Argonne, Illinois

and

Wladyslaw J. Swiatecki

Lawrence Radiation Laboratory
University of California
Berkeley, California

August 30, 1962

I. INTRODUCTION

In this part, we present the results of quantitative studies of the properties of saddle point shapes of a uniformly charged drop possessing a sharp surface.[1] Within the idealization adopted in the present series of papers the total potential energy of the drop is made up of two parts, the electrostatic and surface energies. The dimensionless parameter x, defined by

$$x = \frac{(\text{charge})^2}{10\,(\text{volume})\,(\text{surface tension})}$$

specifies the relative magnitudes of the two energies. The qualitative aspects of a number of families of equilibrium shapes resulting from the balancing of the electric repulsion and the attractive surface tension were discussed in Part IV, to which the present paper serves as a quantitative sequel.

The principal qualitative result of Part IV was that a distinction was drawn between cylinder-like shapes of equilibrium (the Bohr-Wheeler family) for $x \gtrsim 0.7$, and strongly necked-in shapes of equilibrium (the Frankel-Metropolis family) for $x \lesssim 0.7$. A second qualitative result concerned the asymmetric shapes of equilibrium (the Businaro-Gallone family) which were found to appear for $x > x_{BG}$, with x_{BG} estimated to be in the neighbourhood of 0.4 or 0.5. This family governs the stability against asymmetry of the

symmetric saddle-point shapes and provides a distinction between fission and spallation.

The discussion in Part IV indicated that it was not certain whether the distinction between the cylinder-like and necked-in families of symmetric saddle-point shapes was of a qualitative or quantitative nature, i.e., whether the transition from one type to the other was discontinuous in a plot against the fissionability parameter x, or continuous but rapid, so that it occurred within a narrow interval of x values. The balance of the evidence presented there was taken to indicate the first alternative. The quantitative studies described here have clarified this ambiguity and the result is that there is a rapid transition from one type of saddle shape to the other, but that the change is not discontinuous.

Concerning the question of the stability of the symmetric saddle-point shapes against asymmetry, the qualitative discussion given in Part IV has been confirmed and the critical value x_{BG}, where stability against asymmetry is lost and a distinction between fission and spallation disappears, has been determined to be $x_{BG} = 0.39_4$.

The other families of equilibrium discussed in Part IV, corresponding to shapes with more than one neck, are not considered in the present paper[2]

II. DESCRIPTION OF THE CALCULATIONS

The method used to find the shapes of equilibrium of the drop was as follows. The configuration of the drop, assumed axially symmetric, was parametrized in terms of an expansion of the radius vector $R(\theta)$ in Legendre polynomials:

$$R(\theta) = \frac{R_0}{\lambda} \left[1 + \sum_{1}^{N} \alpha_n P_n(\cos\theta) \right] ,$$

where the set of N coefficients α_n specifies the shape, and λ is a parameter normalizing the volume of the drop to the standard value $4/3\ \pi R_0^{\ 3}$ (see Parts III and IV. The highest value of N used in the present calculations was N = 18.) The surface and electrostatic energies of the drop were then calculated by numerical integrations and, for a given value of the fissionability parameter x, the total energy was made stationary with respect to small changes of all α_n's. This was accomplished by a suitable search in the N-dimensional space of the α_n's.

The procedure for tracing out the behaviour of the family of symmetric equilibrium shapes as function of x was usually to start with the known members of this family for x = 1 (a sphere) or x = 0 (two spheres in contact) and to decrease (or increase) the value of x in small steps, using the known shape as a starting point of the search at the new x value. (Once several consecutive solutions had been determined, a more refined extrapolation was used to predict the next unknown shape.) Each time a symmetric shape of equilibrium was determined in this way, its properties were subjected to a detailed study. This included the determination of the shape and its energy (surface, electrostatic, and total), the moments of inertia about different axes, and the quadrupole moment. In addition, the degree of instability of the shape

was determined, i.e., the number of degrees of freedom with respect to which the shape was unstable (see Part IV). This meant the determination of the number of linearly independent combinations of the α_n's with respect to which there was instability. At this stage small deformations with and without reflection symmetry were included, i.e., small changes in all α_n's with n from 1 to N were considered, so that the degree of instability with respect to symmetric as well as asymmetric displacements could be ascertained. A byproduct of this study was the determination for each shape of equilibrium of those linear combinations of the α_n's that make the potential energy in the vicinity of the saddle a sum of squares (without cross terms of the type $\alpha_n \alpha_m$). The number of negative terms in this sum is the degree of instability of the shape in question, the coefficients in the sum are proportional to the elastic constants of the shape, and the linear combinations of α_n's that make the potential energy a sum of squares are the eigenvector displacements associated with the elastic constants. The distortions of the drop corresponding to the eigenvector displacements are not invariant with respect to a change of the expansion parameters α_n to another set, and their significance is, therefore, only relative to the particular choice of the expansion parameters (in our case coefficients in an expansion of the radius vector in Legendre polynomials). The number of negative elastic constants (and thus the degree of instability) is, however, an invariant (1) and is a fundamental intrinsic property of each shape of equilibrium. It follows also that the critical value of x at which an elastic constant changes sign does not depend on the particular parametrization of the shape in terms of Legendre polynomials but is an intrinsic property of the family of equilibrium shapes.

A discussion of the reliability and accuracy of the calculations if given in the Appendix. The situation is roughly that the results are generally very

accurate in the range of x values from 1.0 down to 0.7, moderately accurate from 0.7 to 0.5, and of uncertain accuracy, in some respects at least, between 0.5 and 0.30. Difficulties were experienced in obtaining solutions below $x = 0.28$, although in the vicinity of $x = 0$ itself excellent representations of the correct saddle shape (a pair of tangent spheres) were obtained.

III. THE RESULTS

Table I is a comprehensive summary of the properties of saddle point shapes from $x = 1.0$ down to small values of x. It consists of a set of subtables, one for each value of x, as listed on the left. Each subtable consists of four rows to be read from left to right. The format of the subtables is indicated at the head of Table I. The first row gives the nine even α_n's (from α_2 to α_{18}) specifying the symmetric saddle shape, followed by the normalizing factor λ. The next two rows, apart from the last two entries, give sixteen values of the radius vector $R(\theta)$, for θ from 0 to 90 deg, in steps of 6 deg. The last two entries in row 3 give the relative quadrupole moment Q of the shape and an index of accuracy (labeled "R. M. S.") designed as a guide to the reliability of the solution in question. If this number is small compared to unity the solution is accurate (see Appendix A-1 for details). The last row gives ξ, the relative deformation energy in units of the surface energy of the sphere, and B_s and B_c, the surface and electrostatic energies in units of their respective values for the spherical configuration (see Part IV). These are followed by the elastic constants c_2 and c_4 for two principal symmetric distortions and c_1 and c_3 for two principal asymmetric distortions. (The coefficients c_n are related to the 'eigenvalues' λ_n of Part III by $c_n = 2\lambda_n$.) The last three entries give the relative moments of inertia taken about the axis of symmetry and about an axis at right angles,

and the reciprocal of the effective moment of inertia, defined by (2):

$$\mathcal{J}_{eff}^{-1} = \mathcal{J}_{\parallel}^{-1} - \mathcal{J}_{\perp}^{-1} .$$

The unit here is the moment of inertia of the sphere.

Figure 1A shows a number of saddle-point shapes for $x = 0$, 0.3, 0.4, 0.5, 0.6, 0.7, 0.8, 0.9 and 1.0. Figure 1B compares the necked-in shapes for $x = 0.3$, 0.4, 0.5, and 0.6, and Fig. 1C the cylinder-like shapes for $x = 0.7$, 0.8, 0.9 and 1.0. In the first case the overall length of the shapes increases with x, in the second case it decreases. The transition from one type of behaviour to the other is farily rapid, as shown in Fig. 2, where the major and minor axes of the shapes are plotted against x. The transition occurs around $x \approx 0.67$ and is marked, in addition to the reversal of the trend in the overall length of the shapes, by a rapid change in the radius of the neck, which is doubled between $x = 0.6$ and $x = 0.72$.

The deformation energy of the above symmetric configurations is shown in Fig. 3. As discussed in Part IV, the portion of the curve between $x = x_{BG}$ and $x = 1.0$ (with $x_{BG} = 0.39_4$ – see below) represents threshold energies for fission. The part of the curve between $x = 0$ and $x = x_{BG}$ corresponds to saddle shapes with instability in two degrees of freedom (one symmetric and one asymmetric) and does not have the significance of a threshold for any reaction. We note again the different behavior of the curve in Fig. 2 for x below and above about 0.67. In the former case the deformation energy ξ is almost a straight line (not quite – there is actually a point of inflexion at $x = 0.54_7$). In the latter case the threshold energy is closely represented by a constant times $(1 - x)^3$. The transition from one trend to the other occurs within a few hundredths of a unit around $x = 0.67$. A simple formula that reproduces approximately the calculated values of ξ may be written as follows:

$$\xi = 0.38\left(\frac{3}{4} - x\right), \text{ for } \frac{1}{3} \leq x < \frac{2}{3};$$

$$\xi = 0.83\,(1 - x)^3, \text{ for } \frac{2}{3} \leq x < 1.$$

(As a mnemonic we suggest the name "Three-Four Threshold Formula" for this expression: apart from a single four all the coefficients in the formula can be made up from threes—considering, that is, an eight as made up of a three and its reflection! The numbers Three and Four are themselves suggested by the first few letters of "Threshold Formula." Further properties of interest to numerologists are that the lower limit of validity of the formula may be taken as one-third (or $x = 0.33$), and that the transition from the first to the second expression occurs at $1 - x = 1/3$ (or at $1 - x = 0.33$). The value of ξ at $x = 1 - 0.33$ is 0.030. The formula is accurate to one unit in the third decimal, which means in practice that thresholds calculated will be in error by less than three-fourths of a MeV.)

The approximate distinction between the region for $x < 0.67$ and $x > 0.67$ is reflected also in other properties of the saddle-point shapes. The upper part of Fig. 4 shows a plot of the moment of inertia $\mathcal{J}_\perp$ taken about an axis at right angles to the axis of symmetry and the lower part shows the moment of inertia $\mathcal{J}_{||}$ about the axis of symmetry. Figure 5 shows the reciprocal of the "effective moment of inertia" $\mathcal{J}_{eff}$. Figure 6 shows the behavior of the quadrupole moment.

Figure 7 shows the values of α_n, specifying the saddle-point shapes, as functions of x. We note that down to about $x = 0.7$, α_2 and α_4 are the only coefficients with appreciable magnitudes. Below 0.7 all the higher α_n's come in rather suddenly, and soon even α_{18} is not negligible. The convergence of our calculations as a function of the number of Legendre polynomials retained changes rapidly from excellent for $x \gtrsim 0.7$ to poor for $x \lesssim 0.7$. This is discussed more fully in the Appendix.

Figures 8A and 8B show the stiffness coefficients ("elastic constants") of the saddle shapes against different types of small distortions: Fig. 8A corresponds to the two principal symmetric distortions, and Fig. 8B to the two principal asymmetric distortions. For x values close to 1, the calculated values agree with the elastic constants deduced from expansions in powers of (1 - x) (see Part III).

We note the rather complicated behaviour of the stiffnesses as functions of x. The stiffness c_2 is the only negative symmetric one, and is associated with a division or fission coordinate. The value of c_2 is zero at x = 1 (where the potential energy has a point of inflection as function of the division coordinate α_2) and then becomes negative, reaching a maximum negative value around x = 0.83. The stiffness c_2 then decreases rapidly in absolute magnitude until, quite suddenly, it flattens out at a small negative value, the flattening-out occurring close to x = 0.67. (A change in sign of the stiffness c_2 would have been associated with a "doubling back" of the Bohr-Wheeler family of shapes—see Part IV.)

The next higher symmetric stiffness c_4, associated at x = 1 with a $P_4(\cos\theta)$ type of rippling, decreases until about x = 0.67, and then flattens out at a small positive value. The lowest asymmetric stiffness c_1 is associated with a displacement of the shape along the polar axis (at x = 1, when the drop is spherical, a $P_1(\cos\theta)$ distortion represents such a displacement). The value of c_1, which in an ideal calculation with infinite accuracy would be exactly zero, remains small, though finite, for all values of x. The next higher asymmetric stiffness c_3, associated with the first intrinsic asymmetric distortion (of $P_3(\cos\theta)$ type at x = 1), decreases with decreasing x. The variation is not smooth, a sudden decrease around x = 0.67 being followed by a more gradual one, the sign of c_3 changing at x = 0.39_4.

Below this value of x there are thus two negative stiffnesses, c_2(symmetric) and c_3 (asymmetric).

Figure 9 illustrates the distortions associated with the lowest symmetric stiffness c_2, a fission coordinate. Figure 10 shows an example of the asymmetric distortion associated with c_1, an almost pure shift of the center of mass without intrinsic distortions. The distortion associated with c_3 is illustrated in Fig. 11 for the particularly important case of x = 0.4, where the symmetric saddle point shape (the dashed figure) is about to become unstable against asymmetry. The nature of this asymmetry is indicated by the solid curve in Fig. 11 and may be identified with a "sucking up" of one fragment by the other. Asymmetric shapes, of which the one shown in Fig. 11 is an example, constitute the Businaro-Gallone family of equilibrium configurations discussed in Part IV.

IV. DISCUSSION

These results, although not yet exhaustive and of uneven accuracy, clarify in a quantitative way certain aspects of the potential energy of an idealized charged drop. In particular, the fate of the conventional family of equilibrium shapes, coinciding with the sphere at x = 1, has been traced down to small values of x. The most fundamental property of this family of shapes, its degree of instability, has been found to be 1 from x = 1 down to $x = 0.39_4$, and 2 below $x = 0.39_4$. This defines the range of x values where the conventional family of saddle shapes has the physical significance of a threshold (see Part IV). The nature of the instability that comes in at $x = 0.39_4$ has been determined and found to correspond to an asymmetric degree of freedom, suggesting the sucking-up of one fragment by the other. (At x = 0 the symmetric shape of equilibrium of two tangent spheres is known to be

unstable against such an asymmetric sucking-up.) Assuming that there are no points of bifurcation in the inadequately studied region around $x \approx 0.2$, the only place in the range $0 < x < 1$, where the nature of the conventional family of equilibrium shapes changes fundamentally, is at the bifurcation point $x_{BG} = 0.39_4$. Above this value the symmetric equilibrium shapes are stable against asymmetry and define a threshold energy; below this value they are unstable against asymmetry and do not define a threshold energy.

In addition to the qualitative change in the properties of the conventional saddle-point shapes at $x = 0.39_4$, we have already noted the quantitative changes that take place in the region around $x = 0.67$, where a rapid transition occurs from necked-in to cylinder-like configurations. Viewed against the background of the discussion in Part IV, where a discontinuous transition between the necked-in (Frankel-Metropolis) and cylinder-like (Bohr-Wheeler) families of shapes was anticipated around $x = 0.7$, the present results represent a step back in the direction of the conventional picture of fission, with a continuous family of saddle-point shapes spanning the necked-in configurations at low x and the cylinder-like shapes at high x. In particular, the Bohr-Wheeler family does not "double up" in a plot against x, and there is no second branch of this family with complete stability against all small distortions. Therefore the more extreme modifications of the conventional picture of fission, considered in Part IV, have not been confirmed.

On the other hand the rapid change in the properties of the saddle-point shapes in the neighbourhood of $x = 0.67$, found in this paper, is in line with the semiquantitative estimates of Part IV. Considering the approximate nature of those estimates, we may regard them as not inconsistent with the present quantitative results. The physical reasons for the occurrence of a critical region of charge values in the neighbourhood of $x \approx 0.7$ were

considered in Part IV and were associated with the transition from an essentially two-body process at low x values, where the necked-in form of the saddle shape determines to a large extent the outcome of the division, to a more complicated situation at high x, where the cylinder-like (or spheroidal) saddle shape does not determine the characteristics of the disintegration.

The present results have made the nature of the distinction clearer, and the following conclusions are suggested. Below about $x \approx 0.67$ the fission of an idealized drop would be relatively simple, with many general properties of the division determined to a large extent by the saddle shape, which may be approximated by two deformed fragments (for example two spheroids) connected by a thin neck. In particular the number of fragments (two) and their most probable relative sizes (equal) may be predicted with some confidence. Moreover, the average kinetic energy of the fragments after division, and their average internal excitations, should be closely related to the effective separation of the two halves of the saddle shape, and to the distortions of the fragments. A description of more refined features of the division, such as the spreads in the kinetic energies and internal excitations around their average values, could also be attempted on the basis of an analysis of the neighbourhood of the saddle-point configurations. This seems particularly promising since the saddle shapes are in some respects well represented by simple configurations of two spheroids. Configurations of <u>tangent</u> spheroids, whose total energy was minimized with respect to their eccentricities, were considered in Part IV. A somewhat better approximation is obtained by minimizing the energy for two spheroids whose tips are held fixed at a suitable constant separation. The separation that reproduced well the exact threshold energies for $x \lesssim 0.67$ was found to be $(0.2)(4\pi/3)^{1/3} R_0 = 0.3224 R_0$, where R_0 is the radius of the sphere of equal

volume (see Fig. 3). The similarity of the saddle shapes and the two-spheroid configurations is illustrated in Fig. 12 for $x = 0.5$ (a) and 0.6 (b). The energies and shapes of the two-spheroid configurations were obtained from more extensive tables prepared by Milton and Wilber (3).

For x greater than about 0.67, the description of the division of an idealized drop would become more complicated, the essential reason for the complication being the necessity to give an account of the stage of the process between the saddle and the moment of division (scission). This stage becomes rapidly more extended as x increases above about 0.67, and it soon becomes impossible to predict with any confidence, on the basis of the properties of the saddle shape, the relative sizes or even the number of fragments to be expected in the division.

The discussion of the stage between the saddle and scission presents a problem of quite a different nature than the calculation of the static equilibrium shapes with which the present series of papers is concerned. In particular, the dynamics of the process would be involved, and the physical properties of the drop, such as viscosity, determining the nature of the hydrodynamics, would have to be considered. These complications, which would not play an essential role for low x values on account of the committed form of the saddle shapes, would come to the fore at values of x greater than about 0.67.

The following summary of the situation is suggested. For x less than about 0.67 the theoretical description of the fission of a liquid drop promises to be relatively simple and the requirement for further progress is, on the theoretical side, the working out of the consequences implied by the necked-in, two-fragment saddle shapes. The use of the approximation of two spheroids provides perhaps a suitable technique for handling this problem. The real

difficulty in this region of x values lies on the experimental side, the cross sections for observing the fission reaction being relatively small compared with competing processes.

For x greater than about 0.67 the situation is reversed. Accurate and exhaustive experiments on many aspects of fission have been available for a long time and further information may be readily obtained owing to the ease of observing the fission of heavy elements. The real difficulties lie on the theoretical side, where fundamental questions on the nature of the process, such as the dynamical characteristics of the division, have to be explored and settled before a theory of the division can be worked out. In the absence of more fundamental theoretical progress in this difficult region of x values, perhaps the best prospects for a limited advance in our understanding of fission lies in an effort to clarify the situation at the lower x values. This could be achieved, on the one hand, by extending the range and comprehensiveness of the experiments in this region and, on the other, by a fuller working out of the details of the theory, which for x below about 0.67, would appear to be rather clear in its broad features, and amenable to an approximate quantitative treatment.

APPENDICES

A. Numerical Procedures

The calculation of the energies and saddle-point shapes of the axially symmetric liquid drop were carried out on an IBM 7090. In this appendix we describe the method by which the surface and electrostatic energies of a shape parameterized by the α_n's were calculated.[4] We will also explain how the positions of the saddle points in the multidimensional α-space were located.

(1). Calculation of the Surface and Electrostatic Energies

Given a set of the α_n's which parameterizes the shape of the drop in terms of its radius vector $R(\theta)$ by the expression

$$R(\theta) = \frac{R_0}{\lambda} \left\{ 1 + \sum_{n=1}^{18} \alpha_n P_n(\cos\theta) \right\} ,$$

the values of $R(\theta)$ and $dR(\theta)/d\theta$ were numerically evaluated for equally spaced values of the angle θ, where θ ranges from 0 to 180 deg. The volume of the resultant figure was then obtained by numerical integration and used to determine the normalization constant λ. The surface area, and hence the relative surface energy B_s of the normalized shape, was then evaluated. This part of the calculation was carried out with 199 equally spaced values of angle θ. All numerical integrations in these calculations were carried out using a six-point numerical integration scheme.

The calculation of the electrostatic energy was a more time-consuming operation. It was therefore performed for a smaller number of grid points, usually 41.

The value of the electrostatic energy was obtained by first calculating the value of the electrostatic potential at each grid point θ_i on the surface of the shape. This was done by evaluating the following single integral, equivalent to that used by Hill and Wheeler (4):

$$\frac{v(\theta_i)}{v_0} = \frac{3}{4\pi R_0^{\,2}}$$

$$2\int \frac{\rho\left[(\rho_i+\rho)\frac{dz}{d\theta} + (z_i - z)\frac{d\rho}{d\theta}\right] K(k) - \frac{1}{2}\left[(\rho_i+\rho)^2 + (z_i - z)^2\right]\frac{dz}{d\theta} D(k)}{\left[(\rho_i+\rho)^2 + (z_i - z)^2\right]^{\frac{1}{2}}}\, d\theta.$$

Here $\rho = R(\theta)\sin\theta$, $z = R(\theta)\cos\theta$, $\rho_i = R(\theta_i)\sin\theta_i$, $z_i = R(\theta_i)\cos\theta_i$, and v_0 is the surface potential of the original sphere. The elliptic integrals $K(k)$ and $D(k)$ (the latter defined as $[K(k) - E(k)]/k^2$ in standard notation) have as argument the quantity k given by

$$k^2 = \frac{4\rho_i\rho}{(\rho_i+\rho)^2 + (z_i - z)^2}$$

They were evaluated using the approximate representations of Ref. (5).

The relative electrostatic energy B_c was obtained from the expression

$$B_c = \frac{1}{2}\int \frac{v(\theta)}{v_0}\left[\frac{R(\theta)}{R_0}\right]^3 \sin\theta\, d\theta,$$

derived from Eq. (9) in Ref. (6).

If the calculation described above was being performed for a saddle-point shape, additional results were obtained. The curvature κ at each grid point was calculated analytically. For a true shape of equilibrium the quantity

$$\phi(\theta) = \frac{1}{5}\,\kappa(\theta)/\kappa_0 + x\,v(\theta)/v_0$$

should be constant, and should be equal to

$$\frac{1}{5}(B_s - 1) + x(B_c - 1) .$$

(See Part III. The quantity κ_0 is the total curvature of a sphere.)

The quantity $\phi(\theta)$ and its deviation from the correct value were evaluated for each grid point. As an index of accuracy the root-mean-square value of this deviation was calculated. This is the 'R.M.S.' of Table I. This quantity should be close to zero if the saddle point has been correctly described by the set of α_n's.

For the saddle-point shape, the moments of inertia and the quadrupole moment were also obtained. Note that the 'quadrupole moment' Q of Table I is a dimensionless quantity defined by

$$Q = \frac{1}{R_0^5} \int\int\int (3z^2 - r^2)\, d(\text{volume}).$$

It is related to the conventional quadrupole moment, defined by

$$Q_{\text{conventional}} = \int\int\int (3z^2 - r^2)(\text{charge density})\, d(\text{volume}),$$

by

$$Q_{\text{conventional}} = Q(\text{total charge})\, R_0^2/(4\pi/3).$$

2. Location of the Saddle Point

Locating the saddle points in the multidimensional α-space was automatically performed by a rather straightforward numerical scheme. An approximate location of the saddle point was used to define the starting coordinates α_n. Values of the energy in the neighborhood of this location were then computed and a quadratic expression in the coordinates was fitted to these values. The location of the extremum in the energy for this quadratic expression was determined and the calculation repeated using this location as

a better approximation to the saddle point. When this iterative scheme led to changes in each of the coordinates of less than some prescribed amount, the calculation was terminated and the coordinates were assumed to be those of the saddle point.

In order to fit a quadratic expression in n variables it is necessary to have $(n^2 + 3n + 2)/2$ linearly independent evaluations of the function. In our case these were obtained by incrementing each of the n variables by plus and minus a fixed number (2n evaluations), and incrementing the variables in pairs, $(n(n-1)/2$ evaluations). The value of the unincremented point supplied the last term needed. The size of the increment in each variable could be chosen independently. For the results presented here the increments were as follows:

$$\Delta\alpha_2 = \pm 0.02$$
$$\Delta\alpha_4 = \pm 0.02$$
$$\Delta\alpha_6 = \pm 0.01$$
$$\Delta\alpha_8 = \pm 0.01$$
$$\Delta\alpha_{10} = \pm 0.01$$
$$\Delta\alpha_{12} = \pm 0.005$$
$$\Delta\alpha_{14} = \pm 0.005$$
$$\Delta\alpha_{16} = \pm 0.005$$
$$\Delta\alpha_{18} = \pm 0.005$$

After a saddle point had been located, additional results were obtained to determine the behavior of the potential energy surface in the neighborhood of the saddle point. The eigenvalues and eigendirections for the quadratic form that represents locally the energy surface were calculated. In the neighborhood of the symmetric saddle points the quadratic form consists of

two independent parts without cross terms, one for symmetric and one for asymmetric distortions. Both parts were brought to principal axes and the eigendirections and eigenvalues determined.

B. Tests of Accuracy

1. Accuracy of the Numerical Procedures

In order to ascertain the accuracy of the numerical results obtained for a shape specified by a set of α_n's, several test calculations were performed. In each of these cases the dependence of the results on the number of grid points used in the numerical integrations was studied. In certain of these test cases the numerical results could be compared directly with those known from exact solutions.

In the results that follow, the quantity in parentheses refers to the number of grid points used in the calculation of that result.

Of the shapes for which the results are known, the simplest is a sphere. The results of the calculations for this shape are as follows

B_s	1.000000 (99)	1.000000 (199)	1.000000 (Exact)
B_c	0.9999982 (41)	0.9999993 (61)	1.0000000 (Exact).

In this particular case the electrostatic potential on the surface is known. The numerical values for this potential were found to differ from the exact result by less than 1 part in 10^6, when 41 grid points were used.

A spheroid is also a shape for which the results can be calculated exactly (see Part III). A spheroid with a ratio of axes of 0.7 to 1.0 was approximated by the first five even terms in the expansion in Legendre polynomials. Using the formula of Part II, these were found to be

$\alpha_2 = 0.231693$, $\alpha_4 = 0.041883$, $\alpha_6 = 0.007451$, $\alpha_8 = 0.001314$, and $\alpha_{10} = 0.000232$. The results for this shape were as follows:

B_s	1.0213834 (99)	1.0213833 (199)		1.0213836 (Exact)
B_c	0.9886766 (41)	0.9886784 (61)	0.9886786 (81)	0.9886789 (Exact)
$\mathcal{J}_\perp$	1.198668 (41)	1.198651 (61)	1.198649 (81)	1.198650 (Exact)
$\mathcal{J}_\parallel$	0.788372 (41)	0.788374 (61)	0.788374 (81)	0.788374 (Exact)
Quad. Mom.	1.374916 (41)	1.374852 (61)	1.374847 (81)	1.374848 (Exact)

For $x = 0.0$, the saddle-point shape is two spheres in contact. This shape can be represented exactly as $[R(\theta)]^2 = \text{constant}\ (P_0 + 2P_2)$. Using this expression, the results for the numerical calculation were:

B_s	1.260027 (99)	1.259868 (199)		1.259921 (Exact)
B_c	0.892437 (41)	0.892442 (61)	0.892443 (81)	0.892444 (Exact)
$\mathcal{J}_\perp$	2.20491 (41)	2.20487 (61)	2.20486 (81)	2.20486 (Exact)
$\mathcal{J}_\parallel$	0.62995 (41)	0.62996 (61)	0.62996 (81)	0.62996 (Exact)
Quad. Mom.	5.27775 (41)	5.27756 (61)	5.27755 (81)	5.27755 (Exact).

This saddle-point shape can also be represented by an expansion of $R(\theta)$ in Legendre polynomials, the first nine even terms of which are (see Part IV):

$\alpha_2 = 1.25$ $\quad \alpha_4 = -0.375$ $\quad \alpha_6 = 0.203125$

$\alpha_8 = -0.1328125$ $\quad \alpha_{10} = 0.0957031$ $\quad \alpha_{12} = -0.0732422$

$\alpha_{14} = 0.0584106$ $\quad \alpha_{16} = -0.0480042$ $\quad \alpha_{18} = 0.0403671.$

The results of the numerical calculations for this set of α_n's were

B_s	1.259271 (99)	1.259228 (199)		1.259921 (Exact)
B_c	0.892441 (41)	0.892430 (61)	0.892434 (81)	0.892444 (Exact)
$\mathcal{J}_\perp$	2.20366 (41)	2.20483 (61)	2.20486 (81)	2.20486 (Exact)
$\mathcal{J}_\parallel$	0.62995 (41)	0.62998 (61)	0.62997 (81)	0.62996 (Exact)
Quad. Mom.	5.27355 (41)	5.27739 (61)	5.27749 (81)	5.27755 (Exact)

As a further test of the numerical integration schemes, typical saddle-point shapes (those for x = 0.4, 0.6, and 0.8) were selected from Table I, (based on 41 grid point integrations for the electrostatic energy), and their properties were recalculated using 61 and 81 grid points. The results were as follows:

Saddle Shape for x = 0.4

B_s	1.280248 (99)	1.280248 (199)	
B_c	0.815730 (41)	0.815739 (61)	0.815744 (81)
$\mathcal{J}_\perp$	3.90878 (41)	3.90920 (61)	3.90924 (81)
$\mathcal{J}_\parallel$	0.54877 (41)	0.54883 (61)	0.54884 (81)
Quad. Mom.	11.2595 (41)	11.2607 (61)	11.2608 (81).

For x = 0.6

B_s	1.285576 (99)	1.285576 (199)	
B_c	0.809449 (41)	0.809476 (61)	0.809477 (81)
$\mathcal{J}_\perp$	4.17560 (41)	4.17357 (61)	4.17344 (81)
$\mathcal{J}_\parallel$	0.49089 (41)	0.49085 (61)	0.49086 (81)
Quad. Mom.	12.3476 (41)	12.3409 (61)	12.3404 (81).

For x = 0.8

B_s	1.080026 (99)	1.080025 (199)	
B_c	0.95367 (41)	0.95368 (61)	0.95368 (81)
$\mathcal{J}_\perp$	1.61846 (41)	1.61840 (61)	1.61840 (81)
$\mathcal{J}_\parallel$	0.62401 (41)	0.62402 (61)	0.62402 (81)
Quad. Mom.	3.3324 (41)	3.3322 (61)	3.3322 (81)

2. Accuracy of the Multidimensional Search Procedure

The determination of the location of a saddle point in the multidimensional α_n space depends on the assumption that a quadratic expression is an adequate local approximation to the potential energy over the range of the scan defined by the set of $\Delta\alpha_n$'s. The presence of appreciable cubic and higher order terms would show up as a dependence of the results on the scan size $\Delta\alpha_n$. In order to test the results of Table I against inaccuracies arising from this source, the whole calculation was re-run twice, once with all $\Delta\alpha_n$'s doubled, and once with all $\Delta\alpha_n$'s halved. As an illustration of the changes produced in the results, we show in Table II the values of B_s and B_c for the saddle shapes at x = 0.9 through 0.4, as found using the three different scan sizes. No important changes in the solutions are apparent. The total energy ξ, being stationary with respect to small deviations from the saddle point configuration, is even less sensitive to small errors in the location of the saddle and was found to be independent to six decimal places of the scan size $\Delta\alpha_n$.

3. Convergence as a Function of the Number of α_n's

The foregoing analysis of the accuracy of the numerical integrations and search procedures shows that at all x values there is no appreciable uncertainty in the final results arising out of those aspects of the calculations. The question of inaccuracies due to the retention of a limited number of terms in the expansion of the shape in Legendre polynomials is not as clear-cut. The effect of the neglect of higher P_n's may be estimated by studying the convergence of the solutions as a function of the highest retained polynomial, $\alpha_N P_N$. Such solutions were obtained, as function of x, for $N = 2, 4, 6, 8, 10, 12, 14, 16, 18$, i.e., the whole calculation of the symmetric saddle shapes was repeated several times, first in one dimension (α_2), then in two dimensions (α_2, α_4), three dimensions, etc., up to nine dimensions (α_2 through α_{18}), and various aspects of the results were compared. Figure 13 shows the major and minor axes of the saddle point shapes obtained from calculations with varying numbers of α_n's, and Fig. 14 shows a more complete comparison of the convergence of the saddle shape at a particular value of x (equal to 0.5). Table III illustrates the convergence with N of the relative energy ξ, and Table IV is a study of the convergence of the moment of inertia $\mathcal{J}_\perp$. The following conclusions are suggested. For x values greater than about 0.7 the convergence of the results is very satisfactory, the increase in the number of even α_n's beyond four (α_2 through α_8) producing very little effect. The convergence is not uniform, the transition from one to two dimensions producing a large change, but the transition from two to three only a small change. Up to three dimensions (α_2 through α_6) the results exhibit the multiple-valued features discussed in Part IV; the critical region of x being around 0.89 for the one-dimensional solution, around 0.72 in two dimensions, and 0.70 in three. The introduction of α_8 and higher α_n's removes the multiple-valuedness.

The convergence of the solutions below about $x = 0.7$ is quite different than above 0.7, additional α_n's producing small but not rapidly decreasing changes. This results in some uncertainty regarding the true appearance of the saddle point shapes at low values of x. In particular, small-scale features like the size and shape of the neck are probably represented poorly and the trend with x of the neck radius below about $x = 0.4$ is almost certainly in error by an appreciable amount (see Fig. 2). (The inclusion of progressively higher α_n's continues to improve the appearance of the neck–see Fig. 14.) On the other hand, overall features of the saddle-point shapes, such as the moments of inertia and, in particular, the energy, change relatively little with increasing N, even for low values of x. We were especially interested in satisfying ourselves that the fundamental critical quantity x_{BG}, where the loss of stability against asymmetry takes place, does not change much with the addition of higher α_n's. Figure 15 illustrates the result of determining x_{BG} using different numbers of even and odd α_n's. The sequence of estimates, $x_{BG} = 0.398$, 0.389, 0.395, 0.389, 0.394, makes it unlikely that the accepted value $x_{BG} = 0.39_4$ is in error by more than a few units in the third decimal place.

The convergence of the radius vector $R(\theta)$ at several values of θ is further illustrated in Fig. 16 for the saddle-point shape at $x = 0.5$.

ACKNOWLEDGMENTS

We would like to thank Victor Brady and Graham Campbell for assistance with the development of the early versions of the computer programs used in these calculations.

This work was done under the auspices of the U. S. Atomic Energy Commission.

FOOTNOTES

1. The references to Parts I, II, III, IV are as follows: Part I–W. J. Swiatecki, Phys. Rev. 101, 651 (1956); Part II–Phys. Rev. 104, 993 (1956); Part III–Paper No. P/651, Proceedings of the Second United Nations International Conference on the Peaceful Uses of Atomic Energy, Geneva, 1958 (United Nations, Geneva, 1958); Part IV–S. Cohen and W. J. Swiatecki, Ann. Phys. 19, 67 (1962).

2. We are indebted to V. M. Strutinskiĭ, N. Ya. Lyashchenko and N. A. Popov for sending us a preprint of their paper, entitled "Symmetric Figures of Equilibrium of a Nucleus with a Sharp Surface," which we received after completion of the present calculations. We shall not attemp to discuss here the relation of their results to ours.

3. The moments of inertia were also calculated independently by Frank Plasil (2), using our sets of α_n's. We are grateful to him for the opportunity of comparing the results of the two methods, which were found to be in agreement.

4. These calculations could also be carried out for other parameterizations. In particular, for the saddle point at $x = 0.0$ the expansion of the square of $R(\theta)$ in terms of Legendre polynomials is more suitable, since only two terms, P_0 and P_2, are then required to represent the exact saddle-point shape.

REFERENCES

1. H. Lamb, "Hydrodynamics," 6th Ed., Dover Publications, 1945, Chap. 11, Para. 377.
2. F. Plasil, Lawrence Radiation Laboratory, Chemistry Division Annual Report, UCRL-10023, January 1961.
3. J. C. D. Milton and B. M. Wilber (unpublished results).
4. D. L. Hill and J. A. Wheeler, Phys. Rev. 89, 1102 (1953).
5. C. Hastings, Jr., "Approximation for Digital Computers," Princeton University Press, Princeton, New Jersey, 1956.
6. S. Frankel and N. Metropolis, Phys. Rev. 72, 914 (1947).

TABLE I

Properties of saddle-point shapes as a function of the parameter x.

x	α_2	α_4	α_6	α_8	α_{10}	α_{12}	α_{14}	α_{16}	α_{18}	λ
	R(0°)	R(6°)	R(12°)	R(18°)	R(24°)	R(30°)	R(36°)	R(42°)	R(48°)	R(54°)
	R(60°)	R(66°)	R(72°)	R(78°)	R(84°)	R(90°)			Q	R.M.S.
	ξ	B_s	B_c	c_2	c_4	c_1	c_3	$\vartheta_{\parallel}$	$\vartheta_{\perp}$	$1/\vartheta_{eff.}$
x = 1.00	0.0000	0.0000	0.0000	0.0000	0.0000	0.0000	0.0000	0.0000	0.0000	1.0000
	1.0000	1.0000	1.0000	1.0000	1.0000	1.0000	1.0000	1.0000	1.0000	1.0000
	1.0000	1.0000	1.0000	1.0000	1.0000	1.0000			0.0000	0.0000
	0.00000	1.00000	1.00000	0.0000	1.2593	0.0000	0.6122	1.0000	1.0000	0.0000
x = 0.98	0.0430	0.0007	0.0000	0.0000	0.0001	0.0001	0.0001	0.0000	-0.0003	1.0004
	1.0433	1.0427	1.0405	1.0367	1.0320	1.0266	1.0202	1.0134	1.0067	1.0002
	0.9940	0.9887	0.9844	0.9811	0.9791	0.9784			0.2215	0.0014
	0.00001	1.00074	0.99963	-0.0148	1.2440	0.0063	0.6028	0.9578	1.0239	0.0674
x = 0.96	0.0901	0.0031	0.0000	0.0001	0.0001	0.0001	0.0001	0.0000	-0.0002	1.0016
	1.0914	1.0898	1.0850	1.0770	1.0668	1.0547	1.0411	1.0267	1.0125	0.9988
	0.9862	0.9753	0.9665	0.9599	0.9559	0.9546			0.4770	0.0014
	0.00004	1.00320	0.99836	-0.0308	1.2201	0.0054	0.5808	0.9135	1.0559	0.1476
x = 0.94	0.1373	0.0069	-0.0002	0.0000	0.0001	0.0001	0.0001	0.0000	-0.0003	1.0038
	1.1396	1.1371	1.1295	1.1171	1.1010	1.0820	1.0608	1.0386	1.0167	0.9960
	0.9770	0.9608	0.9478	0.9382	0.9324	0.9305			0.7477	0.0014
	0.00015	1.00734	0.99618	-0.0552	1.1711	0.0048	0.5530	0.8712	1.0944	0.2340
x = 0.92	0.1827	0.0124	-0.0003	-0.0001	0.0001	0.0001	0.0001	0.0000	-0.0002	1.0068
	1.1867	1.1832	1.1726	1.1555	1.1333	1.1072	1.0783	1.1484	1.0191	0.9916
	0.9669	0.9459	0.9292	0.9170	0.9097	0.9073			1.0224	0.0013
	0.00036	1.01282	0.99323	-0.0675	1.1320	0.0042	0.5242	0.8326	1.1377	0.3221
x = 0.90	0.2298	0.0197	-0.0007	-0.0003	0.0001	0.0001	0.0001	0.0000	-0.0002	1.0108
	1.2353	1.2307	1.2170	1.1949	1.1661	1.1324	1.0952	1.0570	1.0200	0.9856
	0.9550	0.9295	0.9093	0.8947	0.8860	0.8831			1.3231	0.0012
	0.00071	1.01993	0.98932	-0.0821	1.0719	0.0031	0.4960	0.7948	1.1896	0.4176

TABLE I (Continued)

x	α_2 R(0°) R(60°) ξ	α_4 R(6°) R(66°) B_s	α_6 R(12°) R(72°) B_c	α_8 R(18°) R(78°) c_2	α_{10} R(24°) R(84°) c_4	α_{12} R(30°) R(90°) c_1	α_{14} R(36°) c_3	α_{16} R(42°) $\vartheta_{\parallel}$	α_{18} R(48°) Q $\vartheta_{\perp}$	λ R(54°) R.M.S. $1/\vartheta_{eff.}$
x = 0.88	0.2779	0.0289	-0.0012	-0.0007	0.0001	0.0001	0.0001	0.0000	-0.0003	1.0158
	1.2846	1.2789	1.2619	1.2345	1.1988	1.1569	1.1110	1.0641	1.0190	0.9778
	0.9416	0.9118	0.8885	0.8717	0.8618	0.8585			1.6467	0.0012
	0.00123	1.02854	0.98448	-0.0946	1.0014	0.0036	0.4658	0.7585	1.2499	0.5183
x = 0.86	0.3274	0.0405	-0.0018	-0.0012	0.0001	0.0002	0.0001	0.0000	-0.0002	1.0221
	1.3355	1.3286	1.3079	1.2748	1.2315	1.1808	1.1254	1.0694	1.0161	0.9680
	0.9264	0.8926	0.8664	0.8479	0.8369	0.8333			1.9986	0.0011
	0.00197	1.03867	0.97866	-0.0994	0.9394	0.0030	0.4365	0.7236	1.3200	0.6244
x = 0.84	0.3799	0.0548	-0.0026	-0.0023	0.0000	0.0003	0.0002	0.0000	-0.0002	1.0298
	1.3887	1.3804	1.3560	1.3166	1.2652	1.2047	1.1390	1.0730	1.0109	0.9557
	0.9089	0.8713	0.8426	0.8225	0.8107	0.8068			2.3921	0.0011
	0.00296	1.05059	0.97164	-0.1039	0.8601	0.0031	0.4090	0.6894	1.4032	0.7379
x = 0.82	0.4354	0.0724	-0.0035	-0.0039	-0.0001	0.0004	0.0002	0.0000	-0.0002	1.0393
	1.4439	1.4343	1.4057	1.3598	1.2994	1.2283	1.1513	1.0744	1.0031	0.9408
	0.8889	0.8479	0.8171	0.7956	0.7831	0.7790			2.8311	0.0010
	0.00425	1.06428	0.96340	-0.1024	0.7733	0.0031	0.3851	0.6563	1.5011	0.8575
x = 0.80	0.4953	0.0944	-0.0044	-0.0063	-0.0004	0.0007	0.0003	0.0000	-0.0002	1.0511
	1.5025	1.4914	1.4584	1.4052	1.3350	1.2518	1.1620	1.0731	0.9920	0.9224
	0.8657	0.8217	0.7891	0.7666	0.7536	0.7493			3.3319	0.0009
	0.00591	1.08002	0.95368	-0.0981	0.6855	0.0024	0.3620	0.6240	1.6183	0.9846
x = 0.78	0.5615	0.1222	-0.0054	-0.0101	-0.0009	0.0012	0.0005	0.0000	-0.0002	1.0661
	1.5654	1.5526	1.5148	1.4537	1.3723	1.2755	1.1708	1.0682	0.9764	0.8996
	0.8385	0.7919	0.7579	0.7348	0.7214	0.7171			3.9161	0.0009
	0.00798	1.09818	0.94218	-0.0877	0.5918	0.0033	0.3474	0.5925	1.7611	1.1200

TABLE I (Continued)

x	α_2	α_4	α_6	α_8	α_{10}	α_{12}	α_{14}	α_{16}	α_{18}	λ
	R(0°)	R(6°)	R(12°)	R(18°)	R(24°)	R(30°)	R(36°)	R(42°)	R(48°)	R(54°)
	R(60°)	R(66°)	R(72°)	R(78°)	R(84°)	R(90°)			Q	R.M.S.
	ξ	B_s	B_c	c_2	c_4	c_1	c_3	$\vartheta_{\parallel}$	$\vartheta_{\perp}$	$1/\vartheta_{eff.}$
x = 0.76	0.6360	0.1579	-0.0061	-0.0159	-0.0020	0.0020	0.0010	0.0000	-0.0003	1.0852
	1.6334	1.6189	1.5758	1.5058	1.4119	1.2991	1.1769	1.0586	0.9551	0.8711
	0.8061	0.7576	0.7228	0.6993	0.6859	0.6815			4.6083	0.0008
	0.01056	1.11907	0.92861	-0.0742	0.4924	0.0022	0.3343	0.5619	1.9371	1.2633
x = 0.74	0.7231	0.2055	-0.0061	-0.0252	-0.0041	0.0037	0.0019	-0.0001	-0.0005	1.1108
	1.7088	1.6923	1.6433	1.5633	1.4547	1.3227	1.1790	1.0418	0.9255	0.8346
	0.7666	0.7171	0.6821	0.6587	0.6454	0.6410			5.4563	0.0009
	0.01373	1.14342	0.91237	-0.0574	0.3926	0.0023	0.3264	0.5326	2.1608	1.4149
x = 0.72	0.8295	0.2717	-0.0044	-0.0404	-0.0087	0.0066	0.0040	-0.0003	-0.0009	
	1.7940	1.7753	1.7196	1.6281	1.5021	1.3458	1.1744	1.0135	0.8832	0.7866
	0.7170	0.6675	0.6331	0.6104	0.5975	0.5934			6.5331	0.0014
	0.01762	1.17209	0.89272	-0.0392	0.2910	0.0036	0.3186	0.5051	2.4547	1.5723
x = 0.70	0.9662	0.3685	0.0010	-0.0665	-0.0185	0.0123	0.0091	-0.0006	-0.0023	1.2002
	1.8906	1.8695	1.8063	1.7018	1.5550	1.3673	1.1582	0.9667	0.8215	0.7217
	0.6528	0.6049	0.5725	0.5511	0.5390	0.5352			7.9330	0.0035
	0.02236	1.20555	0.86915	-0.0234	0.1908	0.0040	0.2926	0.4820	2.8493	1.7239
x = 0.68	1.1391	0.5031	0.0106	-0.1098	-0.0371	0.0232	0.0199	-0.0013	-0.0058	1.2785
	1.9882	1.9649	1.8946	1.7774	1.6094	1.3845	1.1269	0.8971	0.7379	0.6394
	0.5742	0.5297	0.5004	0.4809	0.4700	0.4668			9.5991	0.0093
	0.02811	1.24006	0.84415	-0.0131	0.1152	0.0053	0.2068	0.4688	3.3334	1.8329
x = 0.66	1.3164	0.6429	0.0142	-0.1640	-0.0574	0.0405	0.0344	-0.0039	-0.0113	1.3675
	2.0562	2.0321	1.9574	1.8325	1.6514	1.3974	1.0942	0.8261	0.6542	0.5597
	0.4994	0.4586	0.4328	0.4153	0.4055	0.4029			10.9924	0.0181
	0.03476	1.26480	0.82572	-0.0112	0.0698	0.0083	0.1439	0.4693	3.7496	1.8640

TABLE I (Continued)

x	α_2 R(0°) R(60°) ξ	α_4 R(6°) R(66°) B_s	α_6 R(12°) R(72°) B_c	α_8 R(18°) R(78°) c_2	α_{10} R(24°) R(84°) c_4	α_{12} R(30°) R(90°) c_1	α_{14} R(36°) c_3	α_{16} R(42°) $\vartheta_{\parallel}$	α_{18} R(48°) Q $\vartheta_{\perp}$	λ R(54°) R.M.S. $1/\vartheta_{eff.}$
x = 0.64	1.4526	0.7417	0.0033	-0.2108	-0.0668	0.0603	0.0450	-0.0092	-0.0165	1.4386
	2.0851	2.0617	1.9864	1.8590	1.6753	1.4095	1.0780	0.7801	0.5958	0.5031
	0.4469	0.4087	0.3852	0.3692	0.3602	0.3580			11.7444	0.0245
	0.04193	1.27670	0.81659	-0.0116	0.0528	0.0110	0.1143	0.4762	3.9809	1.8489
x = 0.62	1.5601	0.8115	-0.0162	-0.2494	-0.0674	0.0798	0.0509	-0.0159	-0.0203	1.4948
	2.0959	2.0737	1.9992	1.8715	1.6898	1.4213	1.0728	0.7515	0.5544	0.4615
	0.4084	0.3722	0.3502	0.3354	0.3270	0.3249			12.1415	0.0276
	0.04937	1.28261	0.81190	-0.0123	0.0419	0.0131	0.0986	0.4837	4.1069	1.8237
x = 0.60	1.6478	0.8612	-0.0413	-0.2806	-0.0612	0.0979	0.0524	-0.0231	-0.0225	1.5401
	2.0977	2.0770	2.0039	1.8769	1.6988	1.4326	1.0746	0.7348	0.5242	0.4291
	0.3785	0.3440	0.3230	0.3093	0.3014	0.2993			12.3410	0.0279
	0.05695	1.28558	0.80947	-0.0127	0.0355	0.0127	0.0995	0.4909	4.1736	1.7977
x = 0.58	1.7272	0.9002	-0.0700	-0.3068	-0.0501	0.1144	0.0503	-0.0302	-0.0230	1.5802
	2.0958	2.0763	2.0048	1.8789	1.7048	1.4431	1.0803	0.7250	0.5003	0.4011
	0.3526	0.3197	0.2994	0.2866	0.2792	0.2771			12.4438	0.0271
	0.06460	1.28720	0.80810	-0.0131	0.0352	0.0139	0.0930	0.4974	4.2109	1.7729
x = 0.56	1.8010	0.9302	-0.1029	-0.3283	-0.0340	0.1289	0.0443	-0.0370	-0.0218	1.6166
	2.0911	2.0727	2.0029	1.8785	1.7086	1.4530	1.0895	0.7214	0.4813	0.3761
	0.3293	0.2980	0.2782	0.2663	0.2593	0.2571			12.4753	0.0286
	0.07229	1.28795	0.80744	-0.0123	0.0234	0.0123	0.0886	0.5036	4.2264	1.7492
x = 0.54	1.8714	0.9518	-0.1406	-0.3451	-0.0124	0.1411	0.0341	-0.0433	-0.0185	1.6500
	2.0840	2.0665	1.9986	1.8762	1.7104	1.4624	1.1020	0.7237	0.4667	0.3531
	0.3074	0.2779	0.2584	0.2474	0.2409	0.2385			12.4471	0.0370
	0.07999	1.28804	0.80736	-0.0112	0.0184	0.0085	0.0778	0.5095	4.2240	1.7258

TABLE I (Continued)

x	α_2	α_4	α_6	α_8	α_{10}	α_{12}	α_{14}	α_{16}	α_{18}	λ
	R(0°)	R(6°)	R(12°)	R(18°)	R(24°)	R(30°)	R(36°)	R(42°)	R(48°)	R(54°)
	R(60°)	R(66°)	R(72°)	R(78°)	R(84°)	R(90°)			Q	R.M.S.
	ξ	B_s	B_c	c_2	c_4	c_1	c_3	$\vartheta_{\parallel}$	$\vartheta_{\perp}$	$1/\vartheta_{eff.}$
x = 0.52	1.9419	0.9633	-0.1867	-0.3554	0.0176	0.1501	0.0177	-0.0485	-0.0123	1.6815
	2.0742	2.0572	1.9912	1.8715	1.7101	1.4716	1.1196	0.7337	0.4570	0.3310
	0.2856	0.2582	0.2388	0.2288	0.2228	0.2201			12.3524	0.0551
	0.08768	1.28751	0.80786	-0.0123	0.0143	0.0086	0.0797	0.5157	4.2018	1.7013
x = 0.50	2.0142	0.9652	-0.2408	-0.3584	0.0555	0.1544	-0.0047	-0.0516	-0.0031	1.7120
	2.0623	2.0452	1.9811	1.8650	1.7078	1.4802	1.1413	0.7512	0.4521	0.3098
	0.2633	0.2383	0.2190	0.2098	0.2044	0.2013			12.2009	0.0817
	0.09535	1.28649	0.80886	-0.0119	0.0112	0.0063	0.0679	0.5220	4.1629	1.6756
x = 0.48	2.0807	0.9531	-0.3001	-0.3513	0.0996	0.1519	-0.0321	-0.0517	0.0084	1.7375
	2.0480	2.0304	1.9682	1.8563	1.7032	1.4874	1.1664	0.7766	0.4544	0.2917
	0.2424	0.2197	0.2005	0.1922	0.1872	0.1839			11.9892	0.1130
	0.10296	1.28499	0.81039	-0.0120	0.0130	0.0076	0.0565	0.5283	4.1061	1.6493
x = 0.46	2.1432	0.9367	-0.3583	-0.3393	0.1428	0.1450	-0.0588	-0.0490	0.0198	1.7610
	2.0341	2.0156	1.9549	1.8475	1.6981	1.4930	1.1901	0.8031	0.4596	0.2761
	0.2226	0.2022	0.1834	0.1756	0.1712	0.1678			11.7716	0.1426
	0.11052	1.28349	0.81199	-0.0116	0.0118	0.0070	0.0481	0.5344	4.0472	1.6242
x = 0.44	2.1982	0.9195	-0.4096	-0.3252	0.1805	0.1354	-0.0820	-0.0446	0.0296	1.7815
	2.0218	2.0022	1.9428	1.8396	1.6933	1.4968	1.2100	0.8272	0.4662	0.2636
	0.2053	0.1867	0.1685	0.1611	0.1572	0.1537			11.5763	0.1674
	0.11801	1.28219	0.81343	-0.0120	0.0111	0.0053	0.0340	0.5397	3.9943	1.6024
x = 0.42	2.2479	0.9030	-0.4558	-0.3107	0.2136	0.1248	-0.1017	-0.0394	0.0377	1.8000
	2.0107	1.9903	1.9318	1.8324	1.6889	1.4997	1.2269	0.8486	0.4731	0.2533
	0.1897	0.1727	0.1553	0.1482	0.1447	0.1413			11.4010	0.1875
	0.12545	1.28107	0.81473	-0.0123	0.0174	0.0052	0.0198	0.5446	3.9468	1.5830

TABLE I (Continued)

x	α_2 R(0°) R(60°) ξ	α_4 R(6°) R(66°) B_s	α_6 R(12°) R(72°) B_c	α_8 R(18°) R(78°) c_2	α_{10} R(24°) R(84°) c_4	α_{12} R(30°) R(90°) c_1	α_{14} R(36°) c_3	α_{16} R(42°) $\vartheta_{\parallel}$	α_{18} R(48°) Q $\vartheta_{\perp}$	λ R(54°) R.M.S. $1/\vartheta_{eff.}$
x = 0.40	2.3014	0.8926	-0.4989	-0.2984	0.2429	0.1145	-0.1185	-0.0339	0.0443	1.8216
	2.0016	1.9802	1.9226	1.8266	1.6855	1.5019	1.2403	0.8658	0.4779	0.2426
	0.1737	0.1581	0.1418	0.1350	0.1319	0.1286			11.2607	0.2038
	0.13284	1.28025	0.81574	-0.0098	0.0180	0.0089	0.0033	0.5488	3.9092	1.5662
x = 0.38	2.3482	0.8806	-0.5372	-0.2846	0.2683	0.1029	-0.1323	-0.0277	0.0494	1.8401
	1.9932	1.9711	1.9141	1.8212	1.6822	1.5034	1.2520	0.8818	0.4839	0.2344
	0.1598	0.1452	0.1300	0.1235	0.1208	0.1177			11.1309	0.2123
	0.14019	1.27951	0.81669	-0.0110	0.0199	0.0126	-0.0101	0.5526	3.8742	1.5515
x = 0.36	2.3915	0.8663	-0.5737	-0.2685	0.2918	0.0897	-0.1443	-0.0207	0.0535	1.8568
	1.9850	1.9621	1.9057	1.8156	1.6789	1.5045	1.2627	0.8976	0.4913	0.2279
	0.1469	0.1329	0.1191	0.1128	0.1104	0.1075			11.0017	0.2158
	0.14750	1.27880	0.81765	-0.0110	0.0216	0.0127	-0.0255	0.5562	3.8393	1.5374
x = 0.34	2.4410	0.8548	-0.6105	-0.2524	0.3140	0.0757	-0.1547	-0.0132	0.0566	1.8767
	1.9775	1.9541	1.8982	1.8107	1.6760	1.5053	1.2720	0.9118	0.4980	0.2211
	0.1328	0.1194	0.1071	0.1011	0.0989	0.0964			10.8881	0.2205
	0.15478	1.27822	0.81848	-0.0098	0.0173	0.0127	-0.0399	0.5595	3.8087	1.5246
x = 0.32	2.4944	0.8427	-0.6478	-0.2336	0.3348	0.0592	-0.1631	-0.0047	0.0584	1.8984
	1.9702	1.9463	1.8910	1.8060	1.6732	1.5058	1.2803	0.9257	0.5056	0.2149
	0.1182	0.1048	0.0943	0.0886	0.0868	0.0847			10.7785	0.2299
	0.16203	1.27768	0.81930	-0.0106	0.0179	0.0125	-0.0530	0.5626	3.7791	1.5127
x = 0.30	2.5464	0.8243	-0.6843	-0.2087	0.3529	0.0387	-0.1682	0.0055	0.0582	1.9185
	1.9624	1.9381	1.8833	1.8007	1.6700	1.5059	1.2882	0.9410	0.5169	0.2119
	0.1044	0.0899	0.0816	0.0762	0.0746	0.0730			10.6585	0.2344
	0.16924	1.27710	0.82023	-0.0116	0.0119	0.0128	-0.0673	0.5657	3.7463	1.5009

TABLE II

Effect of Scan Size on Energies.

x	B_s Half-Scan	B_s Standard Scan	B_s Double Scan	B_c Half-Scan	B_c Standard Scan	B_c Double Scan
0.9	1.019913	1.019930	1.019781	0.989332	0.989323	0.989406
0.8	1.080011	1.080016	1.080242	0.953684	0.953682	0.953540
0.7	1.205279	1.205552	1.205398	0.869347	0.869152	0.869262
0.6	1.285595	1.285578	1.285522	0.809460	0.809474	0.809521
0.5	1.286564	1.286494	1.286403	0.808785	0.808855	0.808946
0.4		1.280248	1.280158		0.815739	0.815851

TABLE III

Energy as a Function of the Number of Dimensions.

x \ Dimension	1	2	3	4	5	6	7	8	9
0.4					0.13524		0.13363	0.13332	0.13284
0.5				0.09881	0.09813	0.09622	0.09618	0.09535	0.09535
0.6				0.05940	0.05922	0.05774	0.05739	0.05719	0.05695
0.7			0.02676	0.02272	0.02251	0.02243	0.02237	0.02237	0.02237
0.8		0.005961	0.005951	0.005907	0.005906	0.005906	0.005906	0.005906	0.005906
0.9	0.001103	0.000712	0.000711	0.000711	0.000711	0.000711	0.000711	0.000711	0.000711

TABLE IV

$\mathcal{G}_\perp$ as a Function of the Number of Dimensions.

x \ Dimension	1	2	3	4	5	6	7	8	9
0.4					3.8749		3.9116	4.0493	3.9092
0.5				4.4211	4.0875	4.2274	4.1716	4.1506	4.1629
0.6				4.3154	4.4699	4.1789	4.2655	4.1651	4.1736
0.7			4.7233	3.0559	2.9265	2.8882	2.8516	2.8515	2.8493
0.8		1.6313	1.6299	1.6188	1.6187	1.6184	1.6183	1.6183	1.6183
0.9	1.3034	1.1897	1.1896	1.1896	1.1894	1.1896	1.1896	1.1895	1.1896

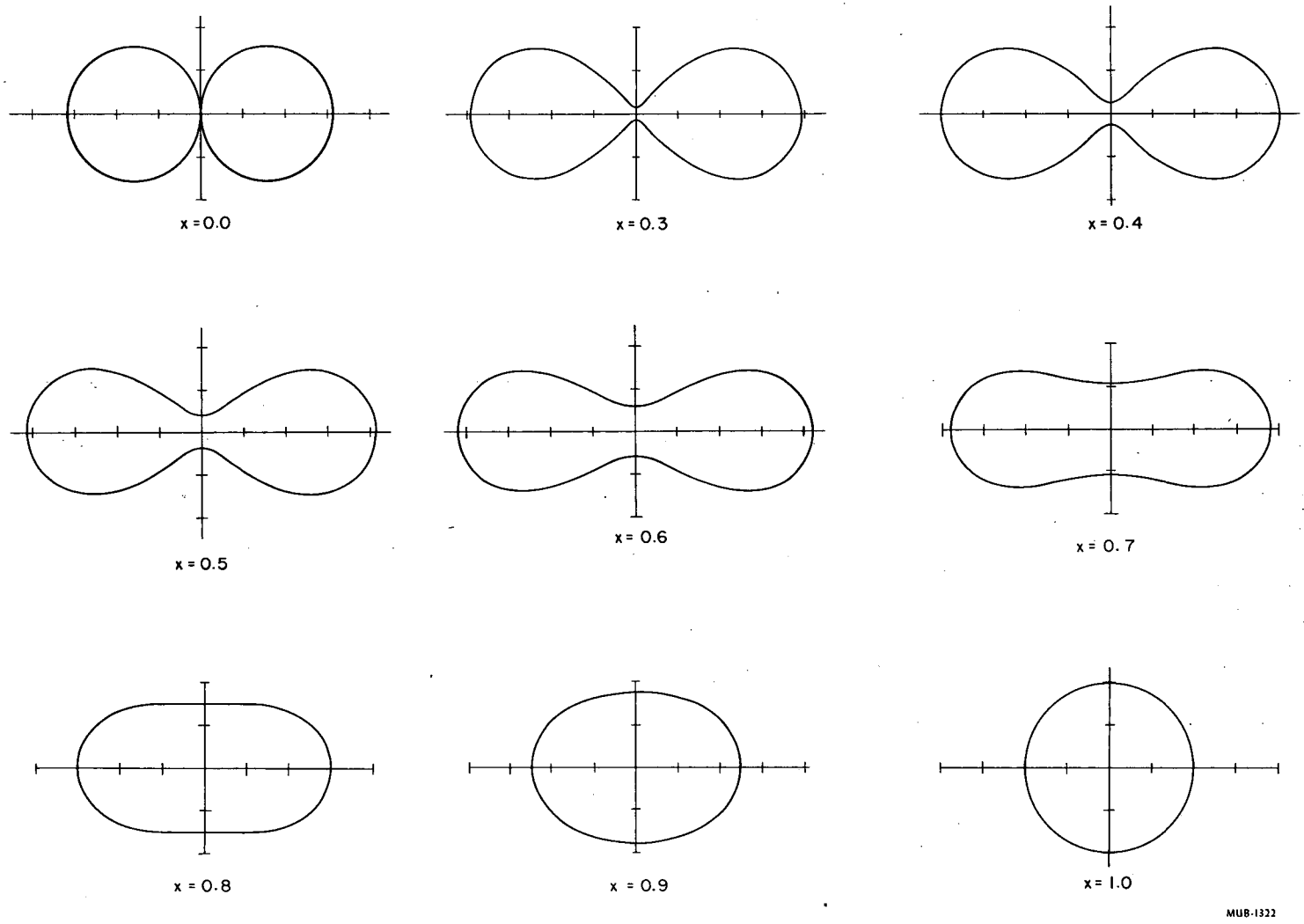

Fig. 1A. Saddle-point shapes for various values of x.

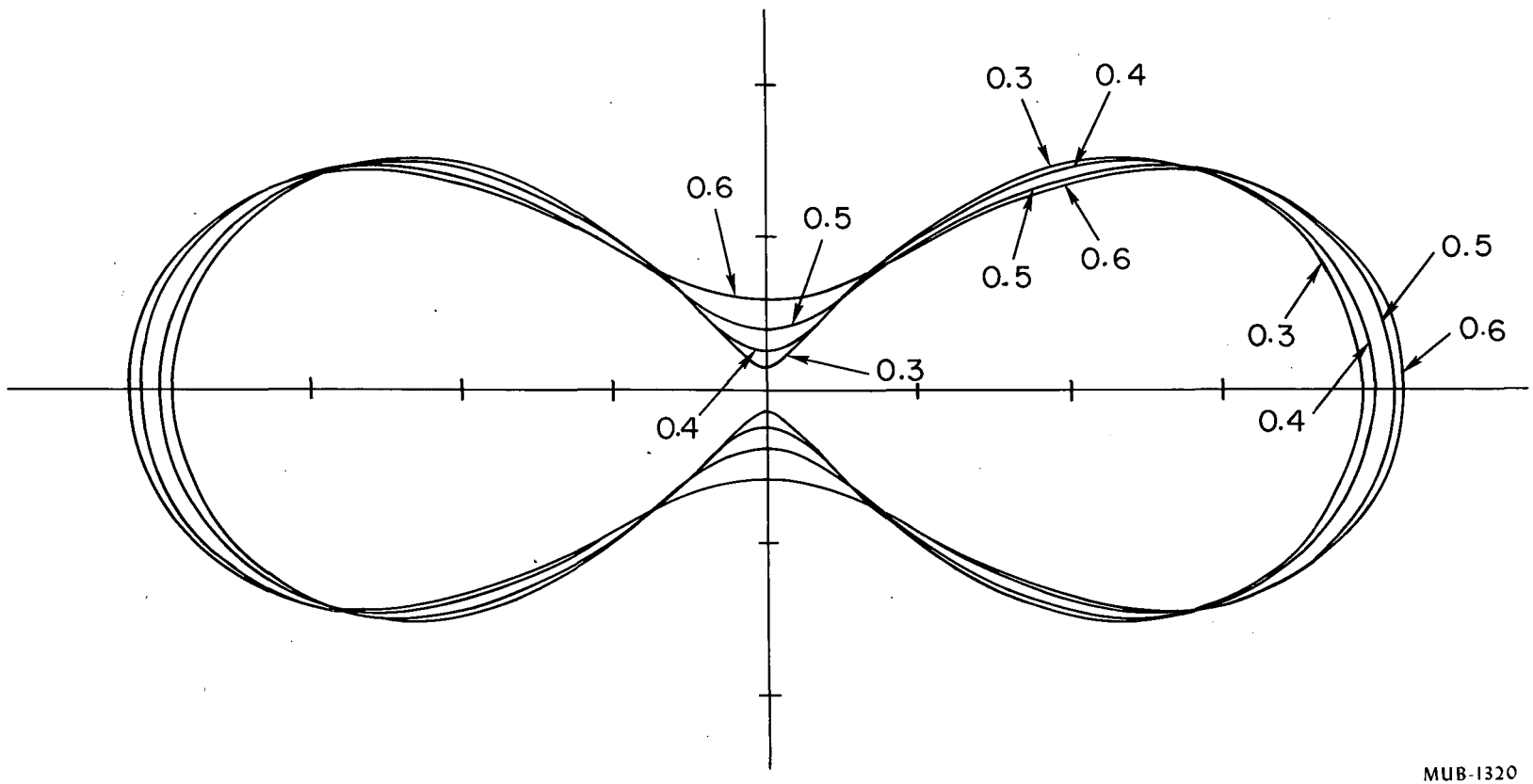

Fig. 1B. Comparison of necked-in saddle-point shapes for $x \leq 0.6$.

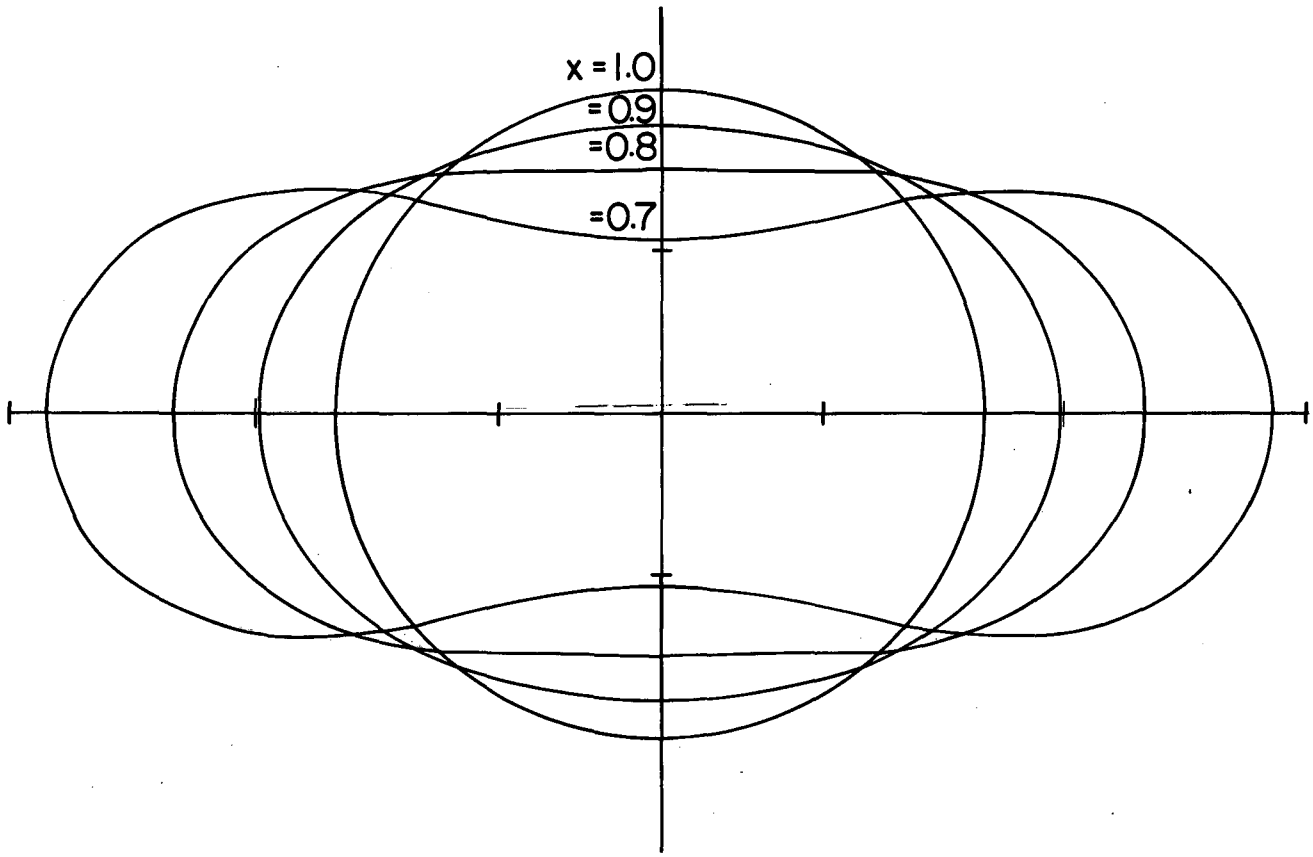

MUB-1319

Fig. 1C. Comparison of cylinder-like saddle-point shapes for $x \geqslant 0.7$.

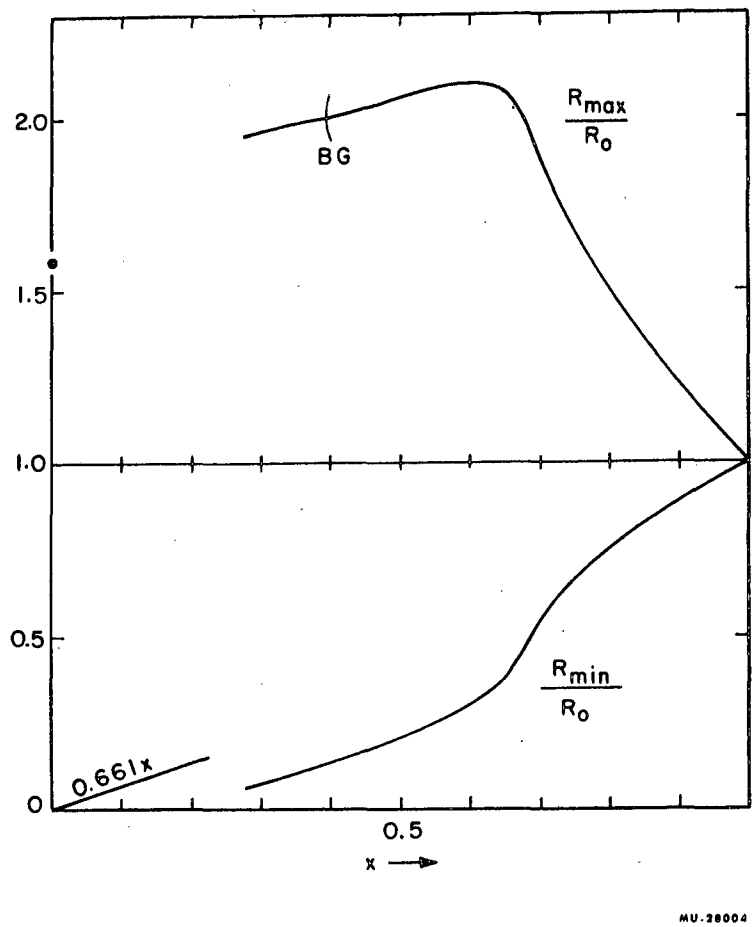

Fig. 2. The behavior of the major and minor axes of saddle-point shapes, as functions of x. The trend in R_{min}/R_0 at small values of x appears to be appreciably in error, as suggested by comparison with the known limiting form for $x \to 0$. The value of R_{max}/R_0 at x = 0 is indicated by a circle. The point where the Businaro-Gallone family of shapes bifurcates at $x = 0.39_4$ has been indicated by BG.

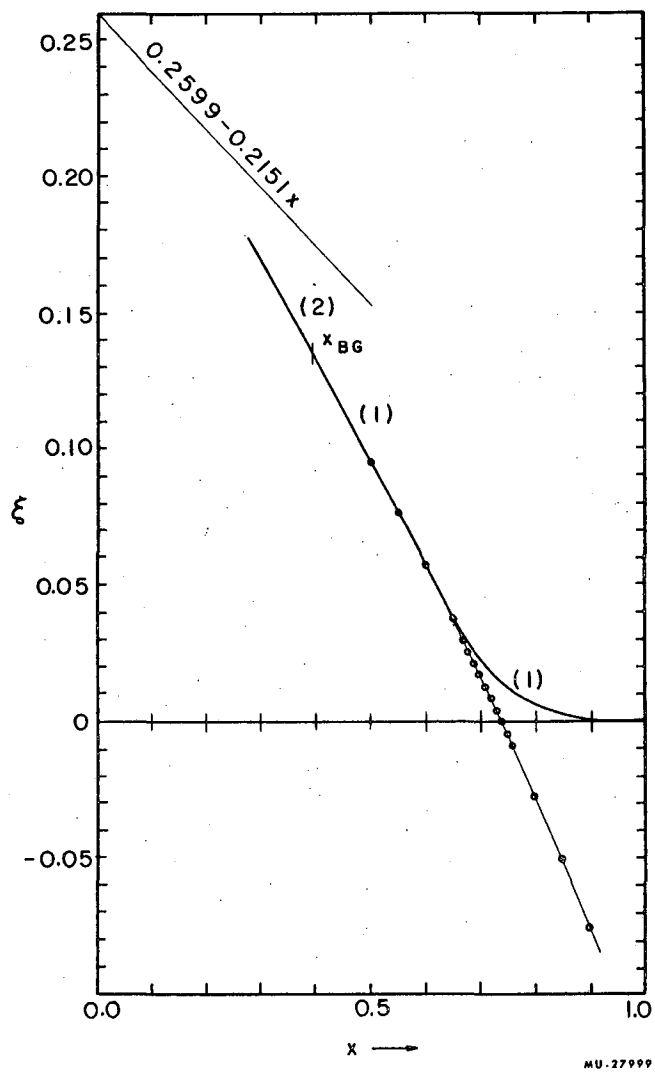

Fig. 3. The relative distortion energy ξ for saddle-point shapes, as a function of x. The numbers in brackets indicate the degree of instability. Threshold energies correspond to the label (1). The transition from an almost linear dependence on x to an almost cubic dependence on (1 - x) occurs close to x = 0.67. The small circles connected by a thin line correspond to the energy of two equal spheroids whose tips are held at a constant separation. The limiting behavior of ξ at small x is indicated.

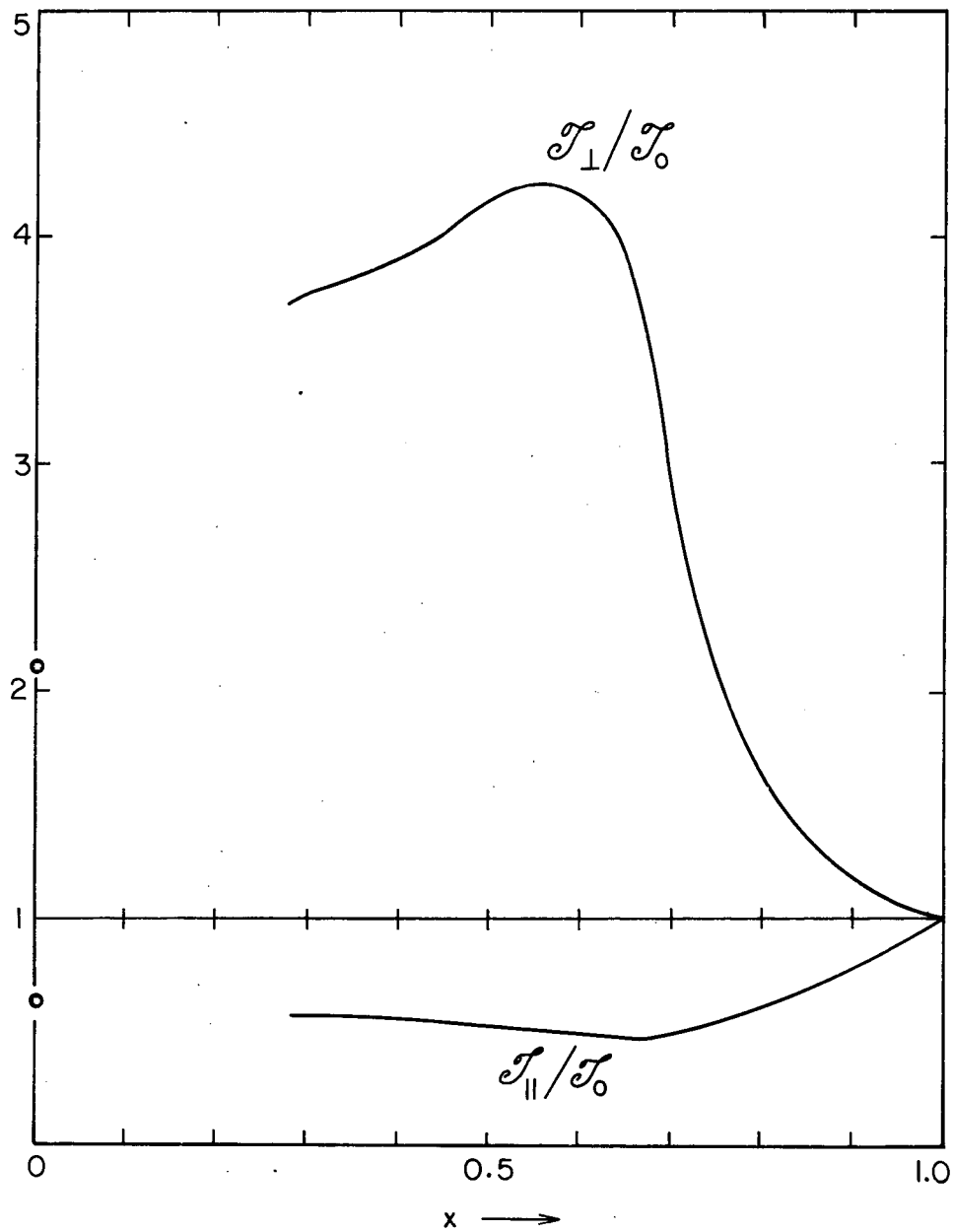

Fig. 4. The moments of inertia about axes parallel and at right angles to the axis of symmetry of the saddle-point shapes are shown as functions of x. The unit is $\mathcal{J}_0$, the moment of inertia of a sphere. Limiting values at x = 0 are indicated by circles.

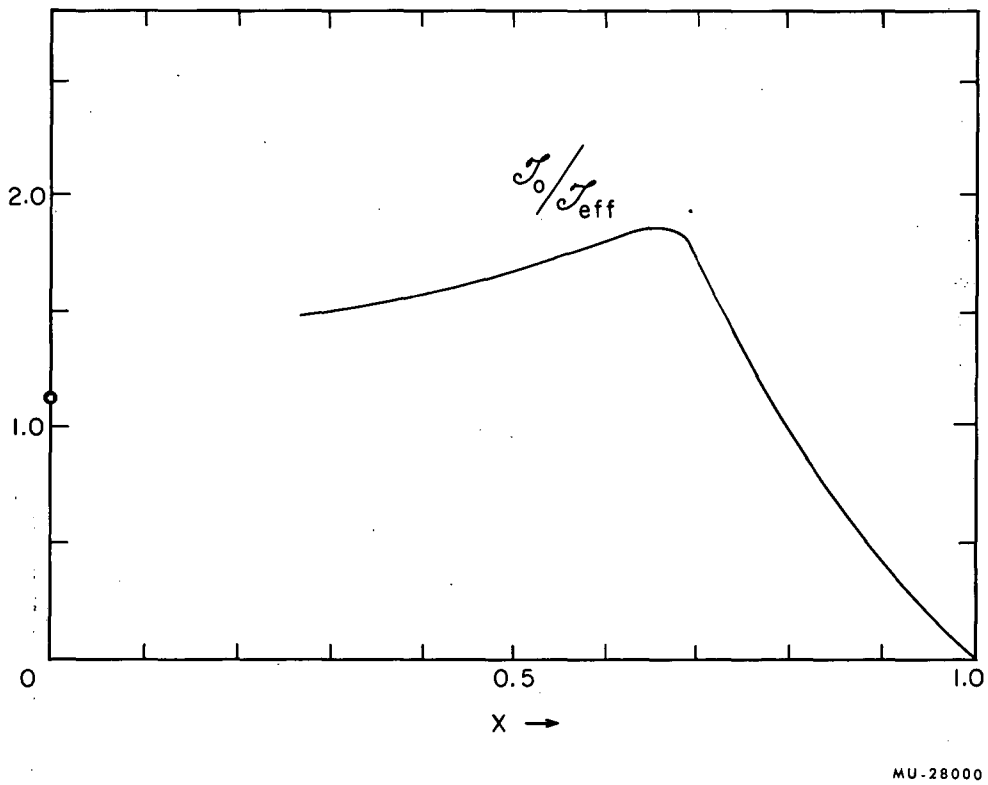

Fig. 5. The reciprocal of the effective moment of inertia $\mathcal{J}_{eff}$, as function of x.

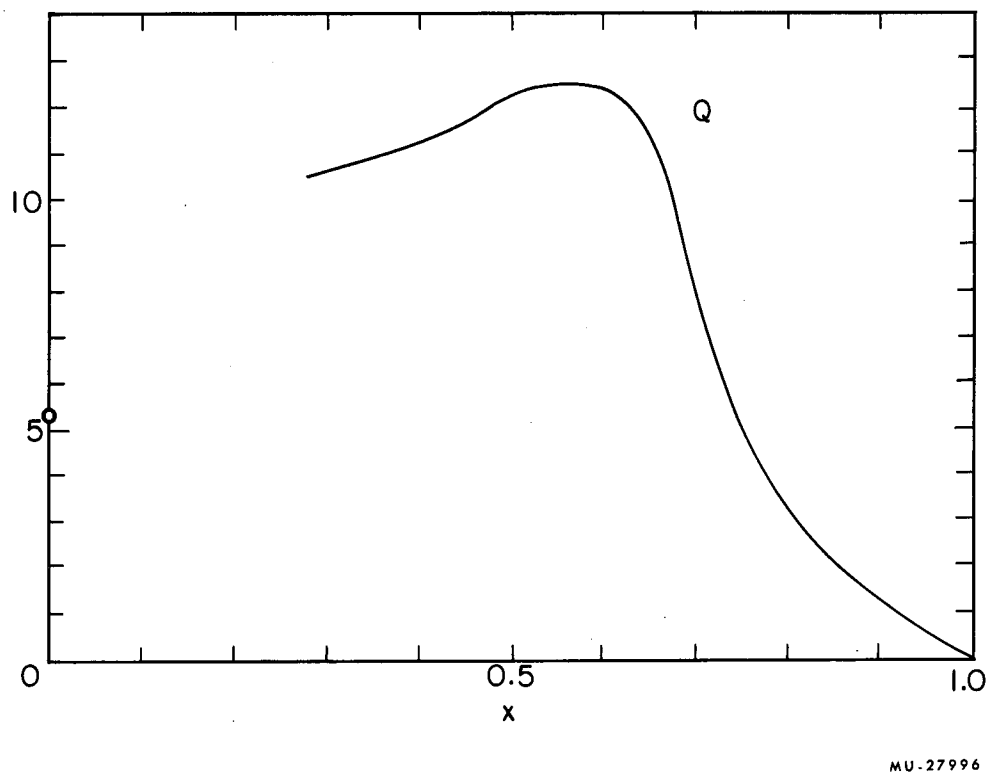

Fig. 6. The relative quadrupole moment Q as function of x. To obtain the conventional quadrupole moment, Q should be multiplied by $(4\pi/3)$ times the total charge on the drop, times the square of R_0 (the radius of the sphere of equal volume).

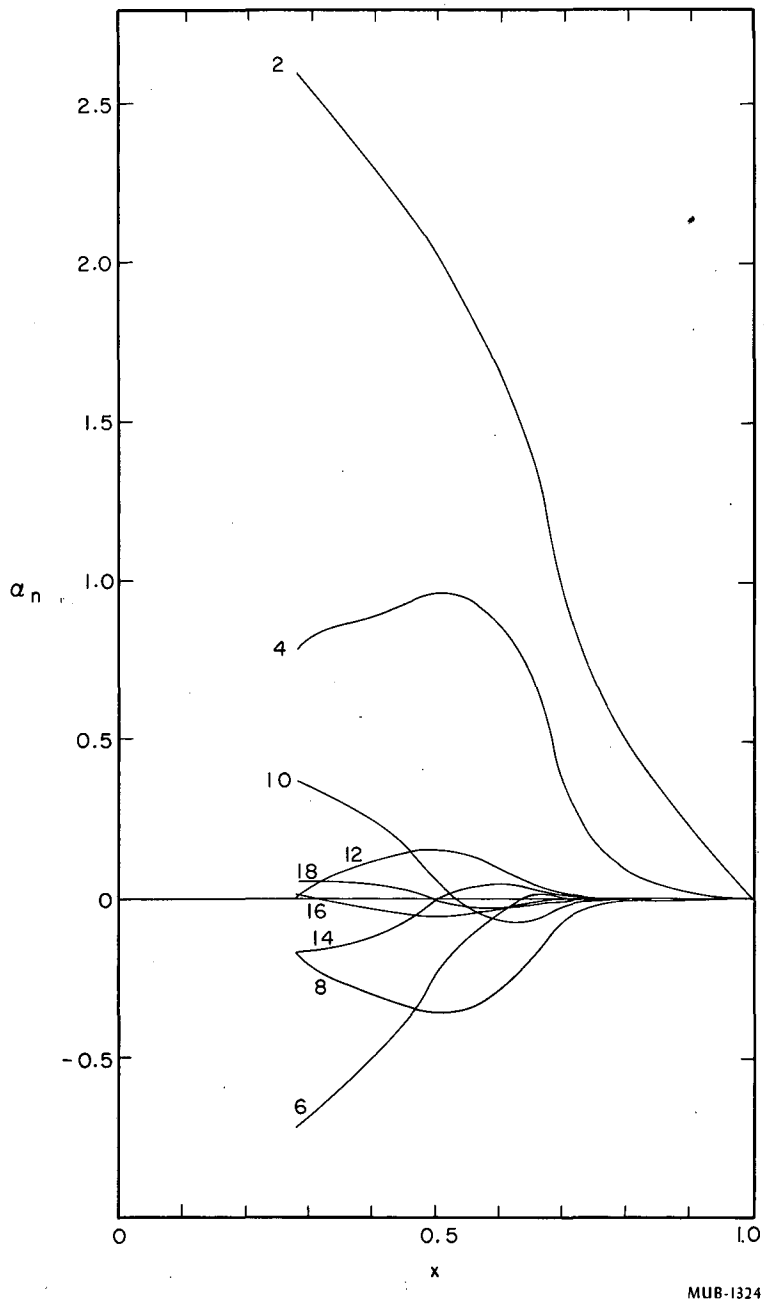

Fig. 7. The values of the expansion coefficients α_n, from α_2 through α_{18}, specifying the saddle-point shapes as functions of x.

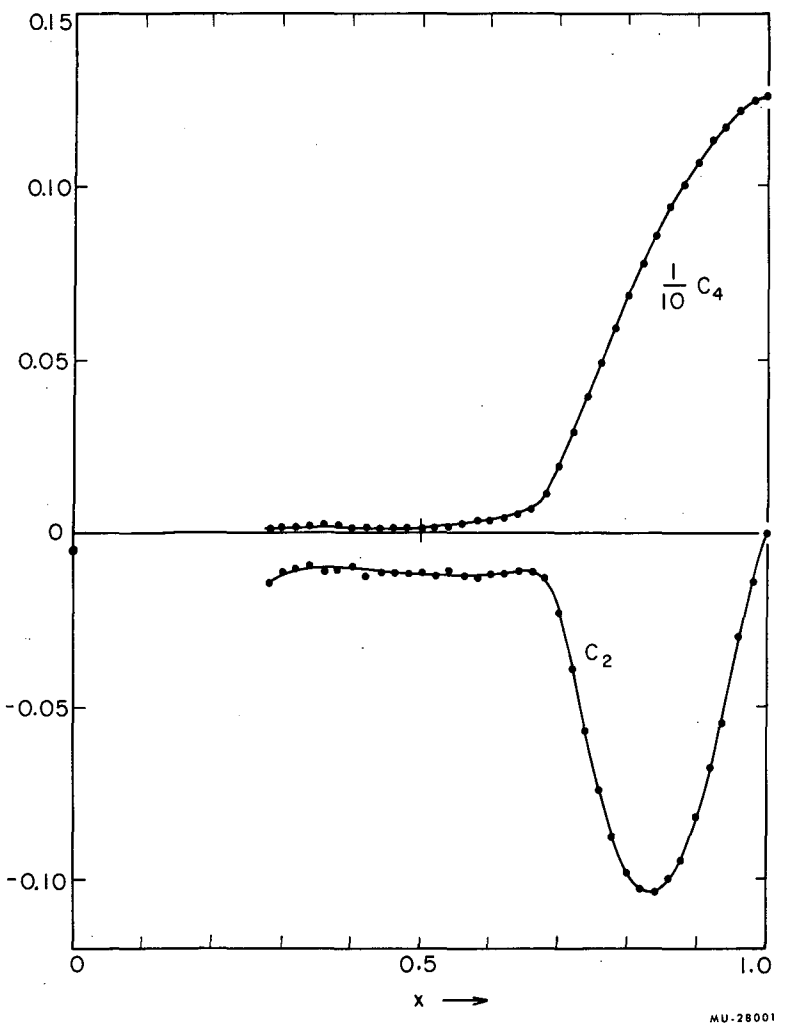

Fig. 8A. The stiffnesses c_2 and c_4, corresponding to symmetric distortions, as functions of x. (Note that c_4 is plotted on a scale reduced by 10.) The slight scatter of the points reflects inaccuracies in the numerical procedures which are beginning to show up in the second derivatives c_n.

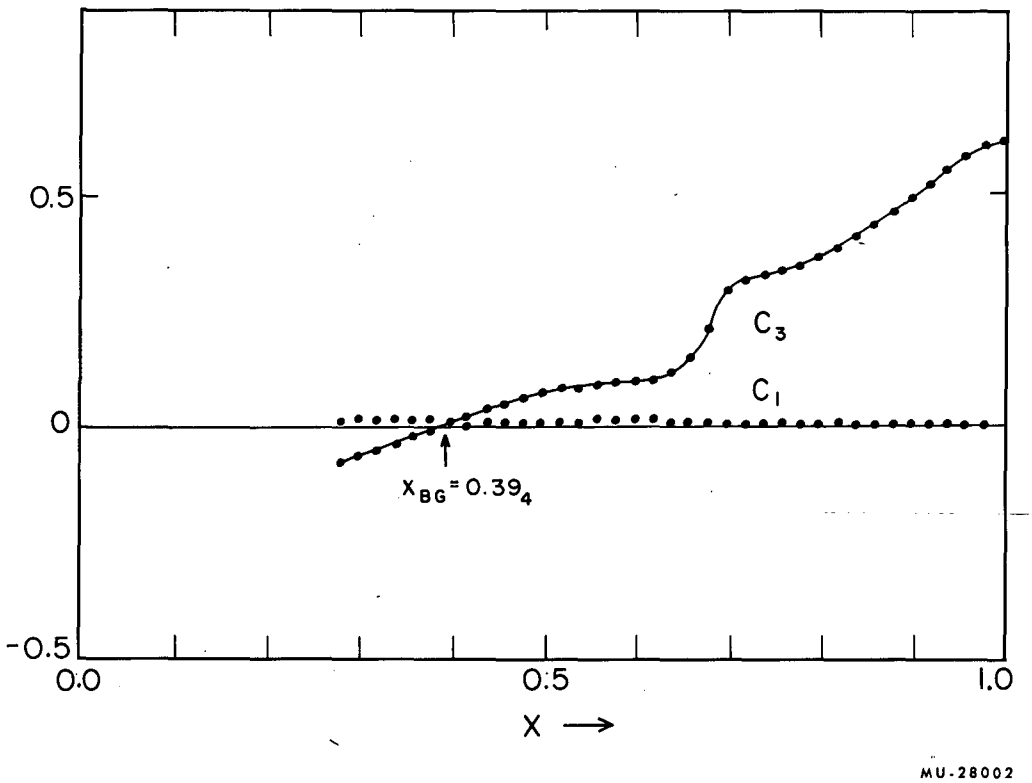

Fig. 8B. The stiffnesses c_1 and c_3, corresponding to asymmetric distortions, as functions of x. Note the complicated behavior of c_3 and the critical point x_{BG}, where c_3 changes sign.

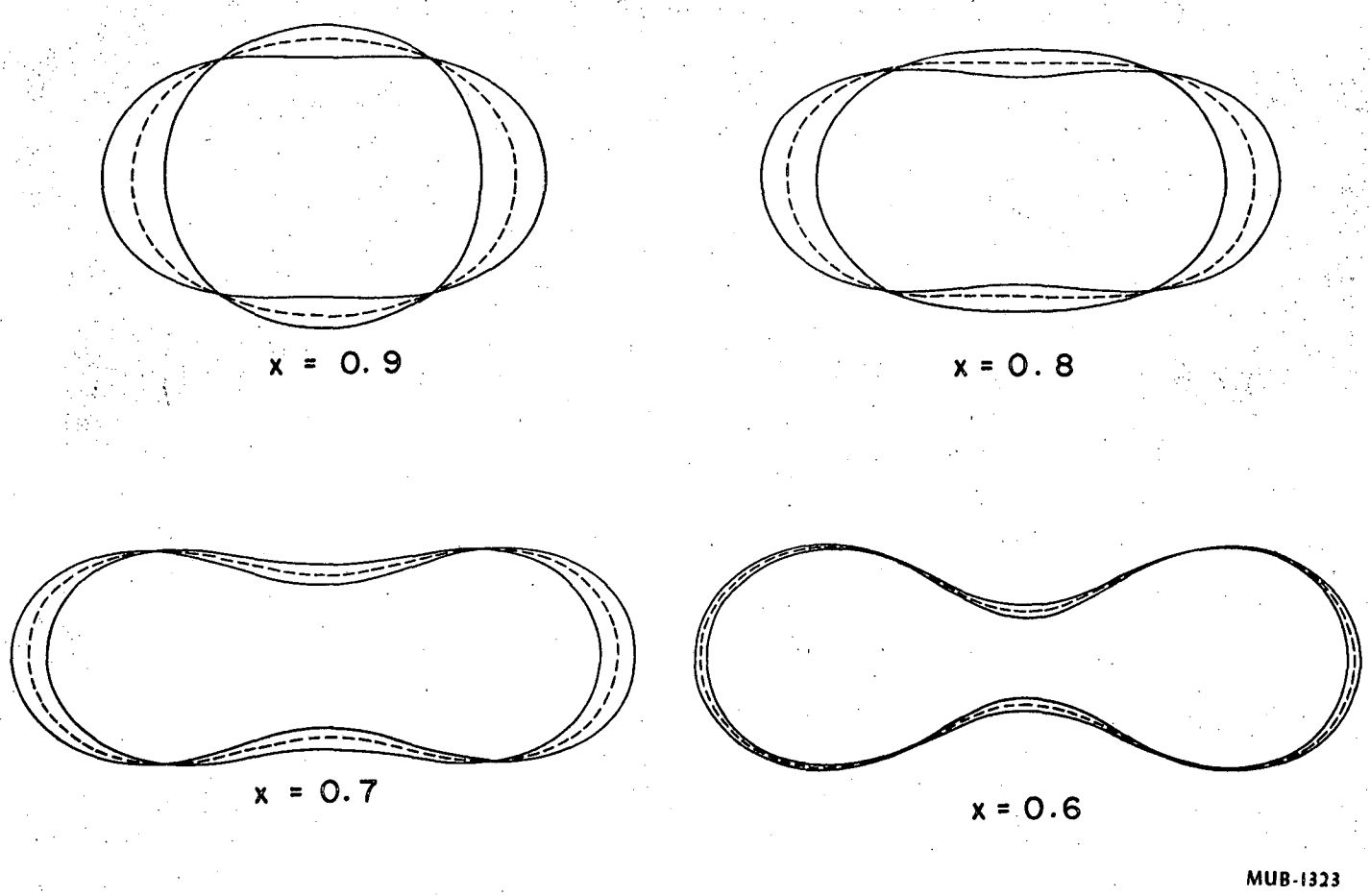

Fig. 9. Examples of distortions associated with c_2, the principal symmetric (fission) coordinate. The saddle shape is shown by a dashed line, and the result of making a positive or negative distortion along the 'fission coordinate' is indicated by the full line. The different cases correspond to x = 0.9, 0.8, 0.7 and 0.6.

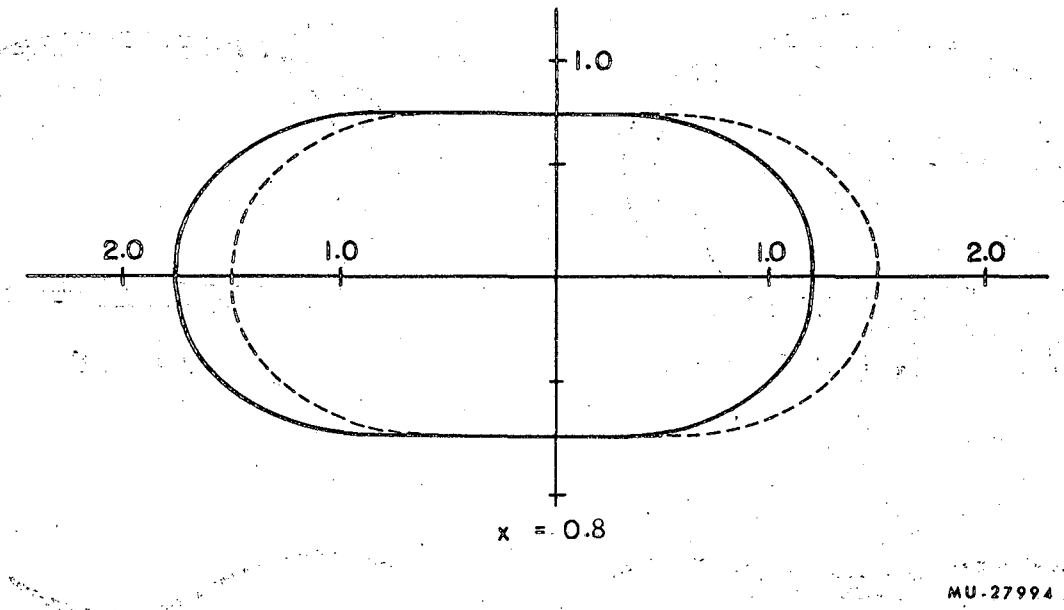

Fig. 10. The asymmetric distortion associated with c_1 (the center-of-mass-shift coordinate).

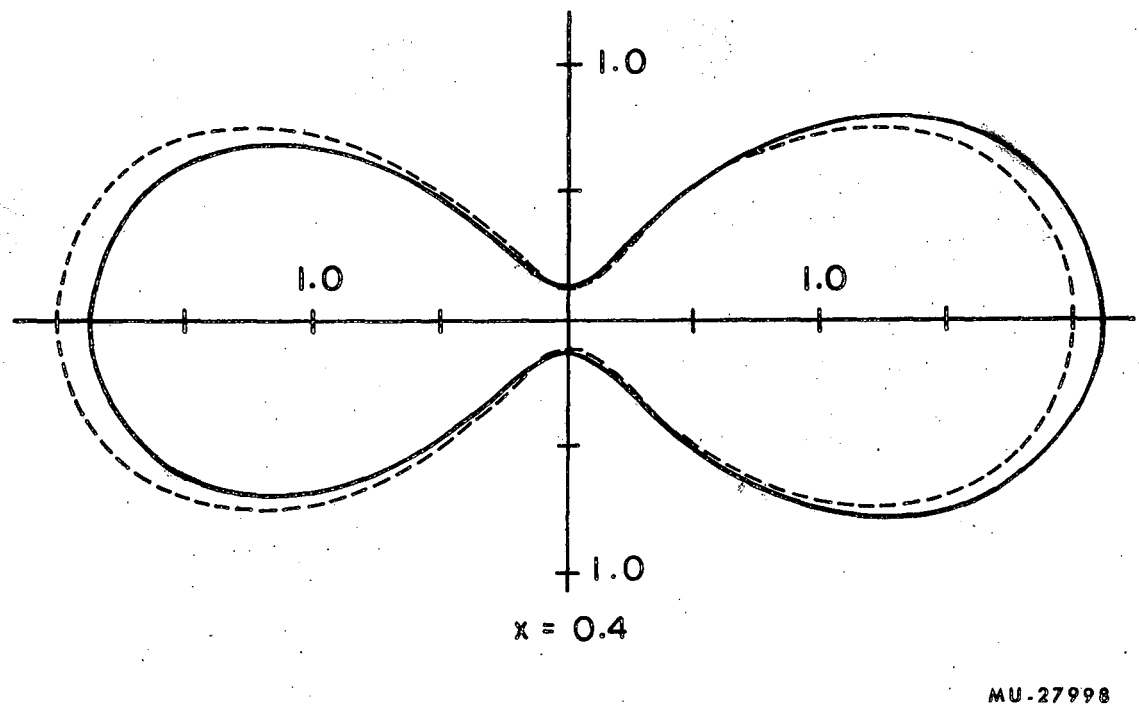

Fig. 11. The asymmetric distortion associated with c_3 - the principal intrinsic asymmetry coordinate. The case illustrated refers to $x = 0.4$, where the symmetric saddle shape (dashed line) is about to become unstable against an asymmetric distortion (solid line). This asymmetric shape is also a member of the Businaro-Gallone family of shapes for x just in excess of the critical value $x_{BG} = 0.39_4$.

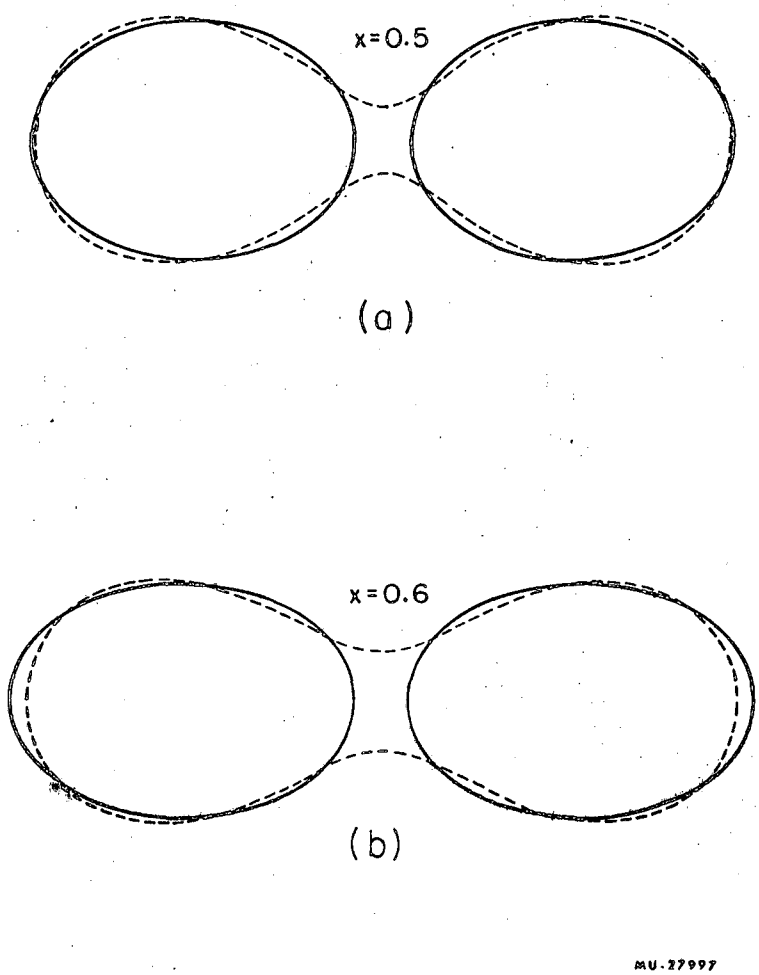

Fig. 12. The saddle-point shapes for x = 0.5 and 0.6 are compared with configurations of two spheroids whose tips were held at a separation of $(0.2)(4\pi/3)^{1/3}\ R_0$, and whose energies were then minimized. The energies of the saddles are 0.0953 and 0.0569, to to be compared with 0.0950 and 0.0572 for the spheroids.

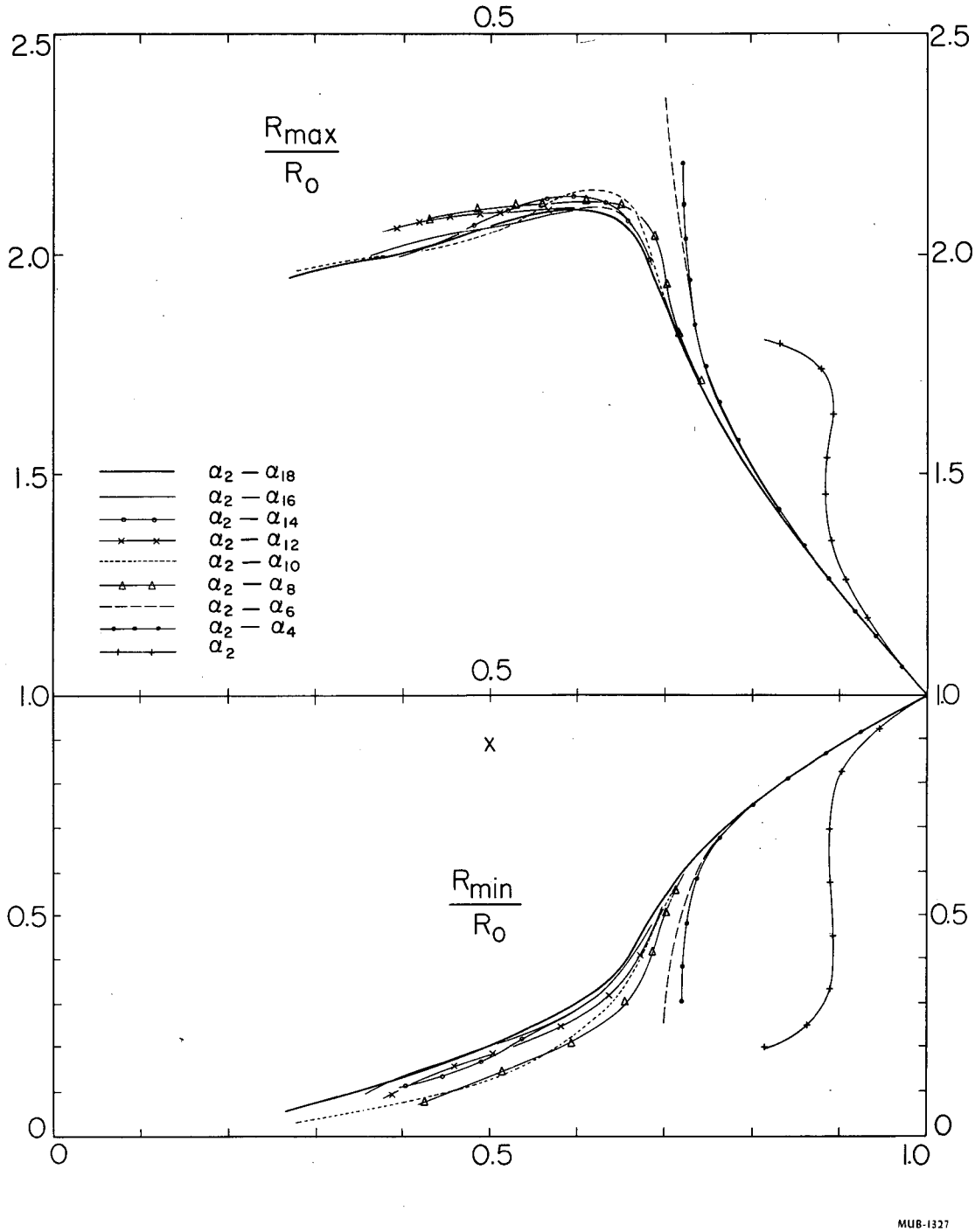

Fig. 13. The convergence of the calculations of saddle-point shapes, with the number of α_n's retained, is illustrated by plots of the major and minor axes of the figures in various approximations.

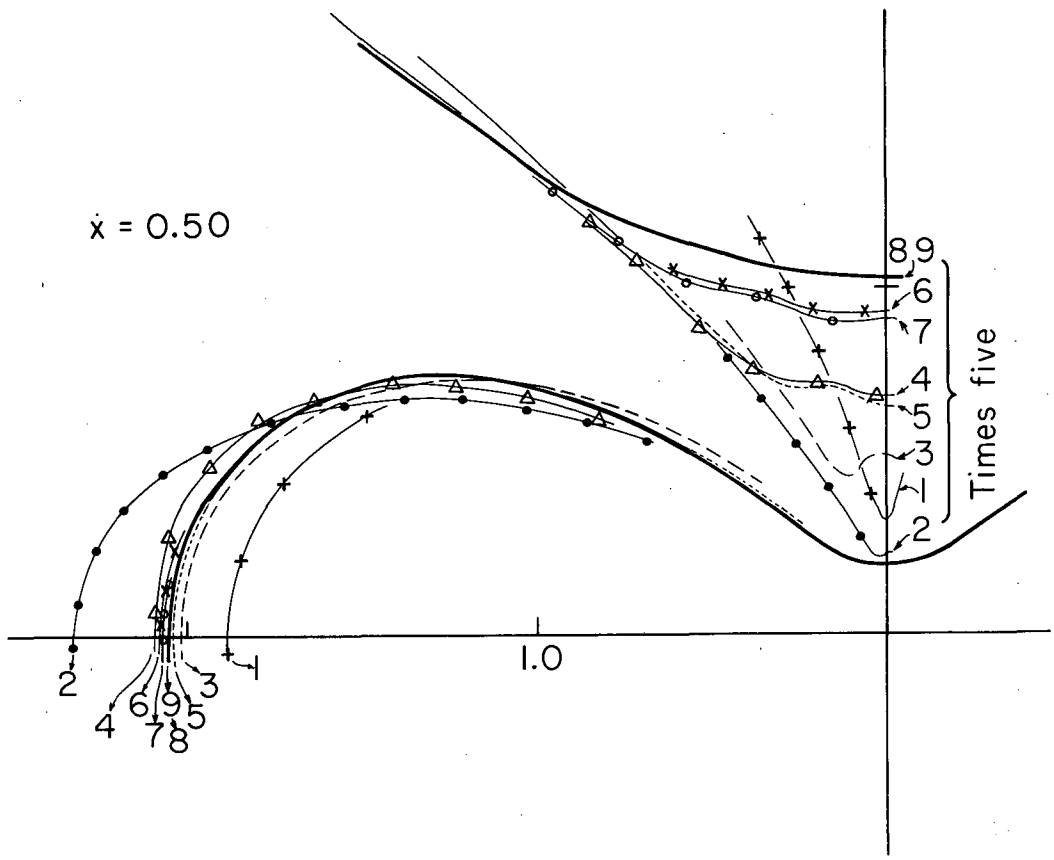

MUB-1328

Fig. 14. The saddle-point shape for x = 0.5 as calculated with different numbers of α_n's. Note that the representation of the neck region improves with the inclusion of higher α_n's, but that Legendre polynomials even beyond P_{18} would probably continue to produce small changes.

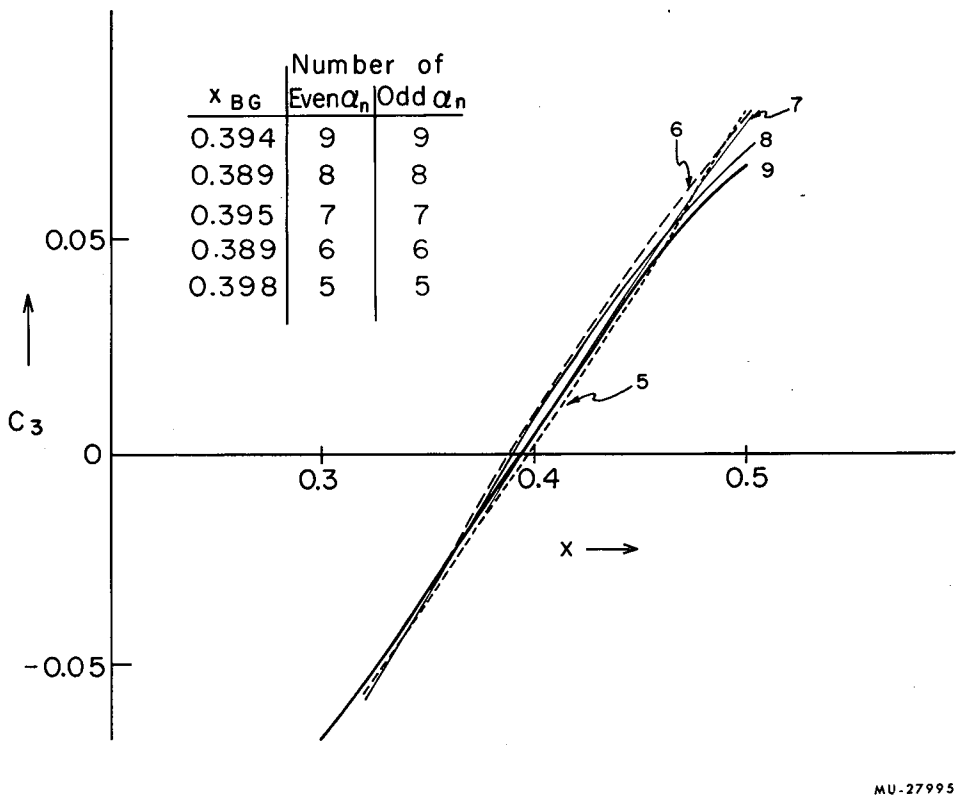

Fig. 15. The determination of x_{BG} from the vanishing of the stiffness c_3 in a plot against x.

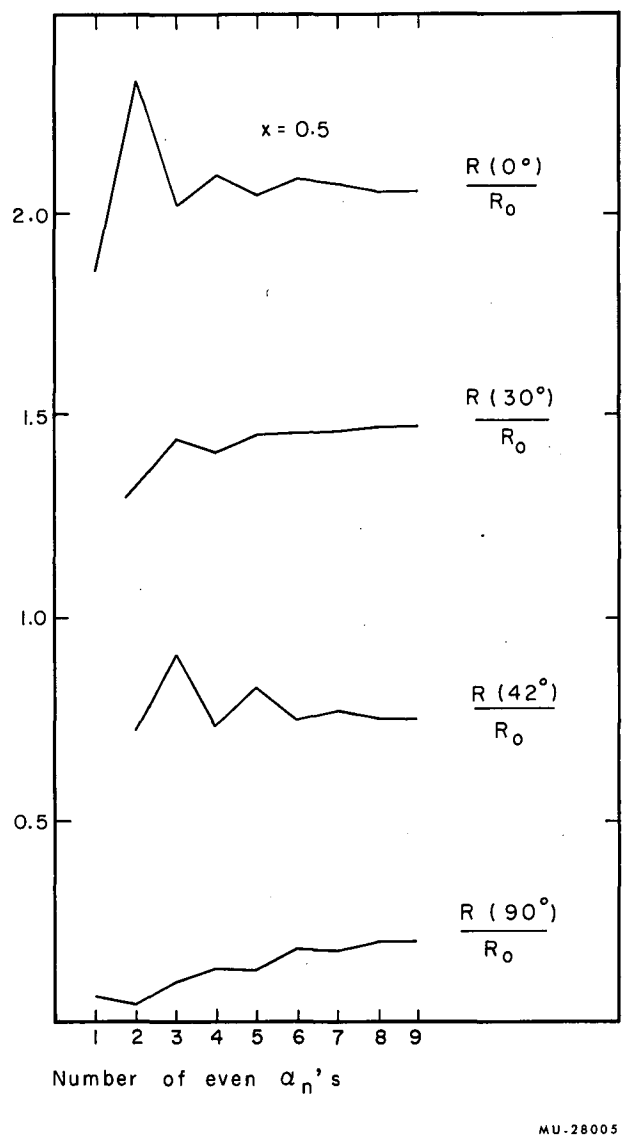

Fig. 16. The convergence of the radius vector at θ = 0, 30, 42 and 90 deg, for x = 0.5. The number of α_n's retained is shown along the abscissa.

This report was prepared as an account of Government sponsored work. Neither the United States, nor the Commission, nor any person acting on behalf of the Commission:

A. Makes any warranty or representation, expressed or implied, with respect to the accuracy, completeness, or usefulness of the information contained in this report, or that the use of any information, apparatus, method, or process disclosed in this report may not infringe privately owned rights; or

B. Assumes any liabilities with respect to the use of, or for damages resulting from the use of any information, apparatus, method, or process disclosed in this report.

As used in the above, "person acting on behalf of the Commission" includes any employee or contractor of the Commission, or employee of such contractor, to the extent that such employee or contractor of the Commission, or employee of such contractor prepares, disseminates, or provides access to, any information pursuant to his employment or contract with the Commission, or his employment with such contractor.